EVOKED AND SPONTANEOUS NEUROTRANSMITTER RELEASES FOR INDEPENDENT SYNAPTIC CURRENTS: MATHEMATICAL MODELING AND ANALYSIS

by

SAT BYUL SEO

Presented to the Faculty of the Graduate School of
The University of Texas at Arlington in Partial Fulfillment
of the Requirements
for the Degree of

DOCTOR OF PHILOSOPHY

THE UNIVERSITY OF TEXAS AT ARLINGTON

July 2017

To My Parents, Kim In Suk and Seo Yong Jae

Who made me who I am.

ACKNOWLEDGEMENTS

I am forever grateful to my supervising professor Dr. Jianzhong Su for attracting me into the field of the mathematical biology constantly motivating, encouraging, and supporting me, and also for his invaluable advice during the course of my doctoral studies.

I would like to thank Dr. Ege Kavalali for his guidance and advice into the computational neuroscience. I wish to thank Dr. Hristo Kojouharov, Dr. Yue Liu, and Dr. Guojun Liao for their interest in my research and for taking time to serve in my dissertation committee. I would also like to thank Dr. David Jorgensen, and Dr. Suvra Pal for their support and giving me helpful guidance in my research, teaching and future. I am especially grateful to Dr. Youngok Kim, Dr. Youngman Nam, and Dr. Joungkyu Kim inspiring and mentoring me to pursue graduate studies in United States. I am grateful to all the teachers who taught me during the years in school in South Korea and in the Unites States.

I also wish to thank my academic brother, Dr. Justin Blackwell for helping and giving me guidance in research. I was lucky to have amazing colleagues, Dr. Hongguang Xi, Gul Karaduman, Mei Yang, Dr. Yousuf Alkhezi, Dr. Pengcheng Xiao, Dr. Byungsoo Moon, Hyungwook Chun, Sl-ghi Choi, and Geoffrey Schuette. I also thank Kilho Shin for helping me to survive in Ph.D life. I would like to truly thank Seul Ki Chang, an amazing pianist and my best friend, for her consistent mentoring.

I would like to express my deep gratitude to my mother, father, and my sister Dan bee for their love, support, and tolerance. I am extremely fortunate to be so blessed. Last, I thank my lovely family and friend with four paws, Oreo, for her love, love, and love.

JULY 10, 2017

ABSTRACT

EVOKED AND SPONTANEOUS NEUROTRANSMITTER RELEASES FOR INDEPENDENT SYNAPTIC CURRENTS: MATHEMATICAL MODELING AND ANALYSIS

SAT BYUL SEO, Ph.D.

The University of Texas at Arlington, 2017

Supervising Professor: Jianzhong Su

Synapses play a major role in neuron communications in the brain. The synapses act through a chemical process called synaptic fusion between pre-synaptic and post-synaptic terminals. Presynaptic terminals release neurotransmitters either in response to action potential or spontaneously independent of presynaptic activity. In the case of glutamate, released neurotransmitters acivate N-methyl-D-asparate (NMDA) and α-3-hydroxy-5-methyl-4-isoxazolepropionicacid (AMPA) receptors within a single postsynaptic site and give rise to miniature postsynaptic currents. In this dissertation, we develop a mathematical model in 3-D to emulate spontaneous and evoked neurotransmissions resulted from glutamate release within a single synapse. We propose numerical methods for solving piecewise continuous heat diffusion equation, estimate and verify its errors of second order accuracy. In order to identify the spatial relation between spontaneous and evoked glutamate releases, we consider

quantitative factors, such as the size of synapses, inhomogeneity of diffusion coefficients, the geometry of synaptic cleft, and the release rate of neurotransmitter, that will affect post-synaptic currents. We conclude quantitatively that as a synapse's size is smaller and if the synaptic cleft space is less diffusive in the peripheral area than the center area, then there is high a possibility of having crosstalk between two signals from spontaneous and evoked releases. On the other hand, when a synaptic size is larger, the cleft space is less diffusive in the central area than the edge area, if the geometry synaptic cleft has a narrower gap in the center and if glutamate release is slower, then there is a better chance for independence of two modes of currents from spontaneous and evoked release. The computed results match well with existing experimental findings and provide a quantitative map of boundaries of physical constraints for having independent synaptic fusion events.

TABLE OF CONTENTS

LIST OF ILLUSTRATIONS

LIST OF TABLES

Table Page

CHAPTER 1

Introduction

My dissertation research is mainly divided into two integrated projects and reflects two aspects of my mathematical work. One is to identify the relationship between two neurotransmissions, spontaneous and evoked transmitter release, one of fascinating questions for neuroscientists during the last half of 20th century, using mathematical modeling with differential equations. The other is to develop numerical methods that can solve the modeling equations with controllable errors, and thus enables to apply this model in neuroscience. We will introduce them in sequential steps in this dissertation.

The structure of this dissertation is as follows. In chapter 2, we introduce concepts of synapses, neurotransmission, and the mechanism how they work in our brains, to understand current research questions. In chapter 3, we review some basic knowledge of mathematical physiology that we should know for our mathematical modeling. In chapter 4, we propose a mathematical model of this synaptic-dynamics. We discuss modeling factors that we will consider including boundary conditions, the geometry of synapse, synaptic size, different diffusion coefficients in the cleft, and the release rate of neurotransmitters from presynaptic terminal. In chapter 5, we work on finite difference methods to approximate solutions to heat equations in the process from presynaptic sites to the cleft. We first show the overview of numerical solutions to the continuous heat equation using finite difference methods, then discuss the situation with piecewise continuous coefficients. In chapter 6, we simulate the process of glutamate release from presynaptic sites into the synaptic cleft to obtain glutamate

molecules concentration at each receptor. In chapter 7, we review numerical methods of system of ordinary differential equations, especially Runge-Kutta methods, that we use to solve our Ordinary Differential Equations(ODEs) system numerically. In chapter 8, we simulate the kinetic process solving a system of ODEs numerically to obtain the opening probability at NMDA receptor. We collect the data of the peak open probability at NMDA receptors at locations opposing evoked release sites or spontaneous release sites when an evoked or spontaneous release occurs. In chapter 9, we define a measurement of independence and suggest two possibilities for small synapses to have less crosstalk from spontaneous and evoked neurotransmitter currents on postsynaptic terminals. In chapter 10, we summarize major findings of our research and discuss our future research plan.

CHAPTER 2

Neuroscience Background

A human brain has over 100 billion neurons, and 90% of the neurons communicate through synapse. A synapse consists of the three components, a presynaptic neuron or terminal, a postsynaptic neuron or terminal, and a synaptic cleft. Networks of neurons and synapse play a key role of communication of electric signals of brain, and are responsible for most of brain functionality. However, there are still many unknown areas for research. In this chapter, we will focus on understanding of synaptic communication, neurotransmission, and their current research questionings.

2.1 What Are Synapses?

Synapses, also known as chemical synapses between neurons, are the main channels of information flow and storage in the brain. Synaptic transmission between neurons is involved in most of what the brain does. When a neuron is active, an electrical impulse travels down its nerve fiber and causes the release of chemical neurotransmitters from its terminal on the presynaptic neuron. The transmitters spread out to a narrow space between pre and post synaptic neurons. The gap is about 20nm wide and is called synaptic cleft. The release neurotransmitters may bind to receptors on the postsynaptic neuron[28]. These chemical neurotransmitters then produce secondary currents in the postsynaptic neuron. We will focus on the chemical synapses in this work. The synaptic cleft consists of fluids, proteins and other molecular obstacles. Presynaptic terminals contain pools of synaptic vessels. They

are small membrane bounded organelles. These vesicles are filled with neurotransmitters mainly in the form of glutamate molecules. When glutamate molecules are released from the presynaptic neuron, they diffuse into the cleft.

2.2 Neurotransmissions, Evoked and Spontaneous Releases

The synaptic fusion releases neurotransmitters into the synaptic cleft. The neurotransmitters mainly consist of glutamate molecules and diffuse in the synaptic cleft, then either bind to specific post-synaptic receptors or flow out of the cleft to extracellular space. Once the neurotransmitters bind to a specific receptor in the postsynaptic membrane, then the receptor channel will open to allow the flux of post-synaptic currents.

The fundamental mechanism for neural communication arises from neurotransmitter releases at synapses. This mechanism originates from the laboratory of Bernard Kats and his colleagues in 1950s[17]. Fast synaptic communication that involves synchronous vesicle fusion evoked by action potential induced Ca^{2+} influx, called evoked release. Alternatively, there is another release of neurotransmitters, called spontaneous release, independent of presynaptic action potentials, and occuring in a random pattern[17]. A crucial observation of these studies that spontaneous neurotransmitter release events tend to occur in discrete quantal packets[17, 8]. Under most circumstances the two forms of release occur concurrently without significant difference in their unitary properties[22, 60]. Spontaneous release typically occurs with a rate of 1- 2 vesicles per minute per release site, whereas evoked release at individual synapses can occur at an extremely high rate, over 100 vesicles per second [19, 40, 50, 51]. However, it was not fully understood if spontaneous neurotransmitter release serves a well-defined purpose until recently[42, 63]. Many neuroscientists has begun to study in spontaneous release and the relation with evoked release.

2.3 More about Spontaneous Synaptic Release

The random synaptic release events typically activate receptors within a single postsynaptic site and give rise to miniature postsynaptic currents, and therefore they have been extremely instrumental in analysis of unitary properties of neurotransmission. In 1994, Murphy and colleagues found that spontaneous miniature glutamate release modulates postsynaptic enzyme activity[27]. Sutton and colleagues showed that minis keep resting protein synthesis in check and respond to stimuli that strengthen synapses by blocking minis and increasing dendritic protein synthesis[57]. More recent works, spontaneous neurotransmission has been mentioned a homeostatic form of synaptic plasticity and induction of synaptic scaling. Spontaneous neurotransmission has an independent role in neuronal communication that is distinct from that of evoked release[24] However, the process of spontaneous neurotransmitter release is still unclear. It has been questioned whether spontaneous release events and evoked release events originate from the same vesicular pathway in presynaptic neurons[4].

2.4 Segregation of Spontaneous and Evoked Neurotransmissions

The relation of evoked and spontaneous neurotransmitter releases and how they are distributed spatially have not been precisely studied due to the lack of direct experimental measurement.

In 2008, David Zenisek found some evidence for the spatial segregation of spontaneous and evoked neurotransmissions that evoked release occurs from ribbon and spontaneous release happens from extraribbon locations in a ribbon-type synaptic terminal, in the goldfish retinal bipolar[61].

Kavalali and colleagues examined the evidence that spontaneous and evoked vesicles originate from different pool of glutamate stores and after releasing, neurotransmitters activate non-overlapping postsynaptic NMDA receptors populations[50, 3, 25].

In 2013, Melom and colleagues showed that even though release probability is not correlated between evoked and spontaneous release of fusion. Neuronal dynamics have two spatially segregated and regulated information channels to induce evoked or spontaneous fusion signals independently[38].

In 2014, Peled and colleagues suggested that although individual synapses can participate in both evoked and spontaneous neurotransmitter release, there is a highly well activated synapse with a preference for only one mode of transmission[46].

In 2015, Schneggenburger and colleagues found that separate functions for Ca^{2+} evoked release and spontaneous transmissions are not necessarily from different origins of two vesicular fusion[52].

From those studies, spontaneous and evoked process are segregated and regulated independently. Many neuroscientist has long recognized the spatial relationship of neurotransmission. But it is unclear how this separation of synaptic currents in NMDA receptors is distributed across individual synapses because of the limited resolution of optical microscopic recording.

2.5 Questioning in Spatial Segregation

How do postsynaptic neurons distinguish evoked and spontaneous neurotransmission and differentially activate postsynaptic signaling? Reese and Kavalali recently showed that two signals from spontaneous and evoked release are not correlated significantly although

spontaneous and evoked release driven NMDA receptor mediated Ca^{2+} transients often occurs at the same synapse[49]. Tang and colleages found how distribution of presynaptic vesicle sites corresponds to the receptors in the postsynaptic neuron. They supported that action-potential -evoked fusion is guided by scaffolding proteins, called nanocolumn, which were likely aligned near the centre of synapses than near the edge. Also this nanocolumn theory proposed that the active zone for evoked vesicle fusion occurs at sites directly opposing postsynaptic receptors[59].

These recent findings indicate that the segregation of sites for spontaneous and evoked neurotransmission with nanoscale subdomains connecting presynaptic and postsynaptic terminals. Therefore, it is possible even for small synapses to possess of this neural functional dynamics.

CHAPTER 3

Preliminaries

3.1 The Law of Mass Action

The fundamental theorem for a chemical reaction is the law of mass action. In this point, "law" means the rate, where chemicals interact to form different chemical combinations. Let two chemicals, A and B, collide with each other to form C as following,

$$A + B \xrightarrow{\text{r}} C. \tag{3.1}$$

The rate of the reaction $\frac{d[C]}{dt}$, is the rate of accumulation of product. The rate is the product of the number of collisions per unit time between two reactants and the probability that a collision is sufficiently energetic to overcome the free energy of activation of the reaction. The number of collisions per unit time is taken to be proportional to the product of the concentrations of A and B with a factor of proportionality that depends on the geometrical shapes and sizes of the reactant molecules and on the temperature of the mixture.

$$\frac{d[C]}{dt} = r[A][B] \tag{3.2}$$

The response 3.2 with the reaction 3.1 is called the law of mass action, and the constant k is the rate constant for the reaction.

We also consider bidirectional reaction as following.

$$A + B \underset{r_-}{\overset{r_+}{\rightleftharpoons}} C, \tag{3.3}$$

where k_- and k^+ denote the forward and reverse rate constants of reaction, respectively. The rate of change of $[A]$ for the reaction 3.3 is

$$\frac{d[A]}{dt} = r_-[C] - r_+[A][B]. \tag{3.4}$$

The quantity A is consumed by the forward direction and generated by the reverse direction.

$$\frac{d[C]}{dt} = r_+[A][B] - r_-[C]. \tag{3.5}$$

At equilibrium, concentration $[C]_{eq} = \frac{r_+}{r_-}[A]_{eq}[B]_{eq}$. If there are no other reaction involving A and C, then $[A] + [C] = C_0$ is constant.

$$[C] = C_0 \frac{[B]}{K_{eq} + [B]}, \tag{3.6}$$

where $K_{eq} = \frac{r_-}{r_+}$ is called the equilibrium constant.

3.2 Diffusion

In order to track of a chemical concentration in space, we must know the mass conservation law. Let u be the amount of chemical species, then the rate of change of u is the sum of local production of u and accumulation of u due to transport.

3.2.1 Conservation Law

Let Ω is a finite region, then

$$\frac{d}{dt}\int_\Omega u \, dV = \int_\Omega f dV - \int_{\partial\Omega} \mathbf{J} \cdot \mathbf{n} \, dA, \tag{3.7}$$

where $\partial\Omega$ is the boundary of Ω and $\mathbf{n}$ is the outward unit normal to the boundary of Ω, f is the local production of u per unit volume, and $\mathbf{J}$ represents the flux of u. If $\mathbf{J}$ is sufficiently smooth, we have this equation by the divergence theorem,

$$\int_{\partial\Omega} \mathbf{J} \cdot \mathbf{n} \, dA = \int_{\Omega} \nabla \cdot \mathbf{J} dV. \tag{3.8}$$

From the conservation law 3.7, we obtain

$$\frac{d}{dt} \int_{\Omega} u \, dV = \int_{\Omega} f - \nabla \cdot \mathbf{J} dV. \tag{3.9}$$

Then we derive the following from 3.9

$$\frac{du}{dt} = f - \nabla \cdot \mathbf{J}. \tag{3.10}$$

3.2.2 Fick's Law

There are many ways to determine the flux $\mathbf{J}$. We will introduce the simplest description the flux of one chemicall species called Fick's law. The flux $\mathbf{J}$ is proportional to the gradient ∇u, but points in the opposite direction since the flow is from space of higher to lower concentration.

$$\mathbf{J} = -D\nabla u. \tag{3.11}$$

The scalar D is the diffusion coefficient, and u represent the heat content of the volume. When Fick's law applies into the conservation equation 3.10, then we obtain the following known as the reaction-diffusion equation.

$$\frac{du}{dt} = \nabla \cdot (D\nabla u) + f. \tag{3.12}$$

3.2.3 Diffusion Coefficients

In the theory of brownian motion from Einstein(1906)[14], a quantitative understanding of diffusion was shown.

If a spherical solute molecule is compared to solvent molecule, then

$$D = \frac{kT}{6\pi\mu a}, \tag{3.13}$$

where k is Boltzmann's constant, T is the absolute temperature of the solution, μ represents the viscosity for the solute, and a is the radius of the solute molecule.

For the non-spherical molecules, Einstein generalized to $D = \frac{kT}{f}$, where f is the Stokes frictional coefficient of the particle.

The molecular weight of a spherical molecule is

$$M = \frac{4}{3}\pi a^3 \rho, \tag{3.14}$$

where ρ represents the molecular density.

Therefore, we rewrite 3.13 in terms of molecular weight as following.

$$D = \frac{kT}{3\mu}\left(\frac{\rho}{6\pi^2 M}\right)^{1/3}. \tag{3.15}$$

For large molecules such as protein, the density is constant nearly 1.3-1.4 g/cm^3, thus $DM^{1/3}$ is almost the same at a fixed temperature for a spherical molecules. The diffusion equation is also known as the heat equation. Next we study the heat equation and its analytic solution.

3.3 Fundamental Solution of Heat Equation

Consider the homogeneous heat equation 3.16 and the nonhomogeneous equation 3.17.

$$u_t - \Delta u = 0, \tag{3.16}$$

$$u_t - \Delta u = f. \tag{3.17}$$

Let $t > 0$ and $x \in \Omega$, where $\Omega \subset \mathbb{R}^n$ is open. The function u is unknown such that $u : \Omega \times [0, \infty) \longmapsto \mathbb{R}$, $u = u(x, t)$. Laplacian Δ is taken with respect to the spatial variables $x = (x_1, x_2, \cdots, x_n) : \Delta u = \Delta u_x = \sum_{i=1}^{n} u_{x_i x_i}$. For the function f in 3.17, $f : U \times [0, \infty) \longmapsto \mathbb{R}$ is given.

Definition 1. *The function*

$$u(x, y, z, t) = \begin{cases} \dfrac{1}{(4\pi t)^{n/2}} e^{-\frac{|x|^2}{4t}} & (x \in \mathbb{R}^n, t > 0) \\ 0 & (x \in \mathbb{R}^n, t < 0) \end{cases}$$

is called the fundamental solution of the heat equation 3.16 for $\Omega = \mathbb{R}^n$.

CHAPTER 4

Mathematical Modeling

4.1 Introduction

For the mathematical goal, we will be modeling of this synaptic-dynamics with the properties in chapter 2. The geometry of synapse, due to small size, has not been described clearly with the limitation of microscopy. We will simulate two modes of neurotransmission, spontaneous and evoked release with different factors and hypotheses including a size, geometry of synaptic cleft, different glutamate diffusion rate in the cleft, and the release rate of neurotransmitters from presynaptic terminals. This modeling may address to the neuroscience question of distribution and separation for two independent spontaneous and evoked release processes and their induced currents in NMDA receptors.

4.2 Geometric Domain

First, we need to set a domain of synaptic transmission. We assume that the cross-section of synapse is 600nm by 600nm for the base model (a large synapse). The geometry for a synapse is a three dimensional array, as shown Figure 4.1a. We define a cubic domain Ω of $1000nm \times 1000nm \times 1000nm$ excluding synaptic terminals. Let S matrix define the domain,

$$S = S(x, y, z) = \begin{cases} 1, & \text{within } \Omega \\ 0, & \text{otherwise} \end{cases}.$$

The pre-synaptic and post-synaptic terminals are simplified as two squares of $600nm \times 600nm$ surface areas facing each other inside Ω. A cleft of $20nm$ of height separates the presynaptic and postsynaptic terminals in our base model.

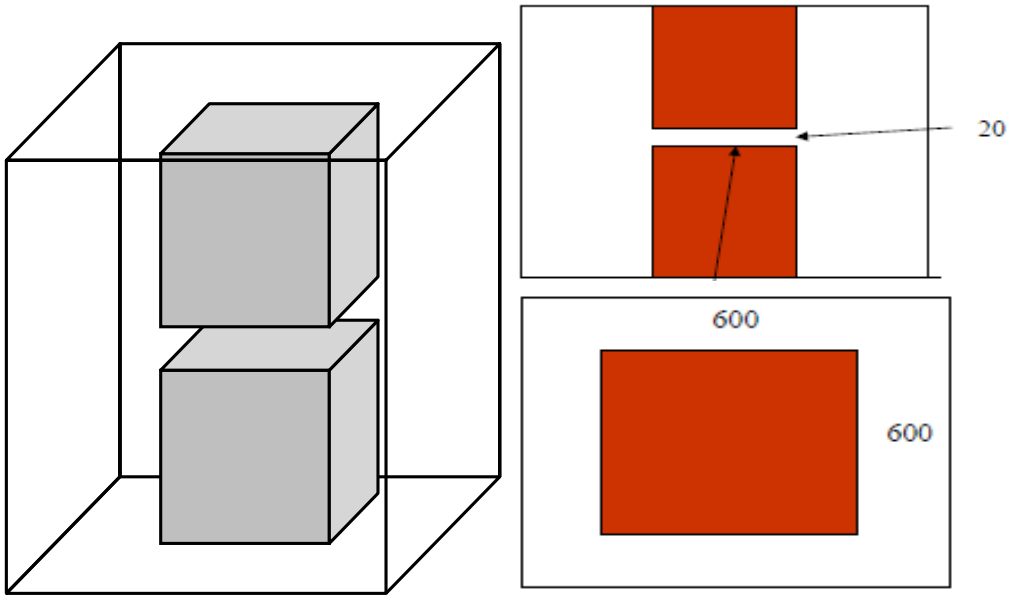

(a) Computational Domain in 3-D (b) Side and Top View

Figure 4.1: Geometric configuration

4.3 Hypothesis of Release Sites on the Presynaptic Neurons

From the neuroscience findings[61, 59], we assume that evoked glutamate release is near the center of presynaptic terminal (a typical location is represented over R6 receptor) and the spontaneous release occurs near the edge(a typical location is represented over R16 receptor) as illustrated in Figure 4.2.

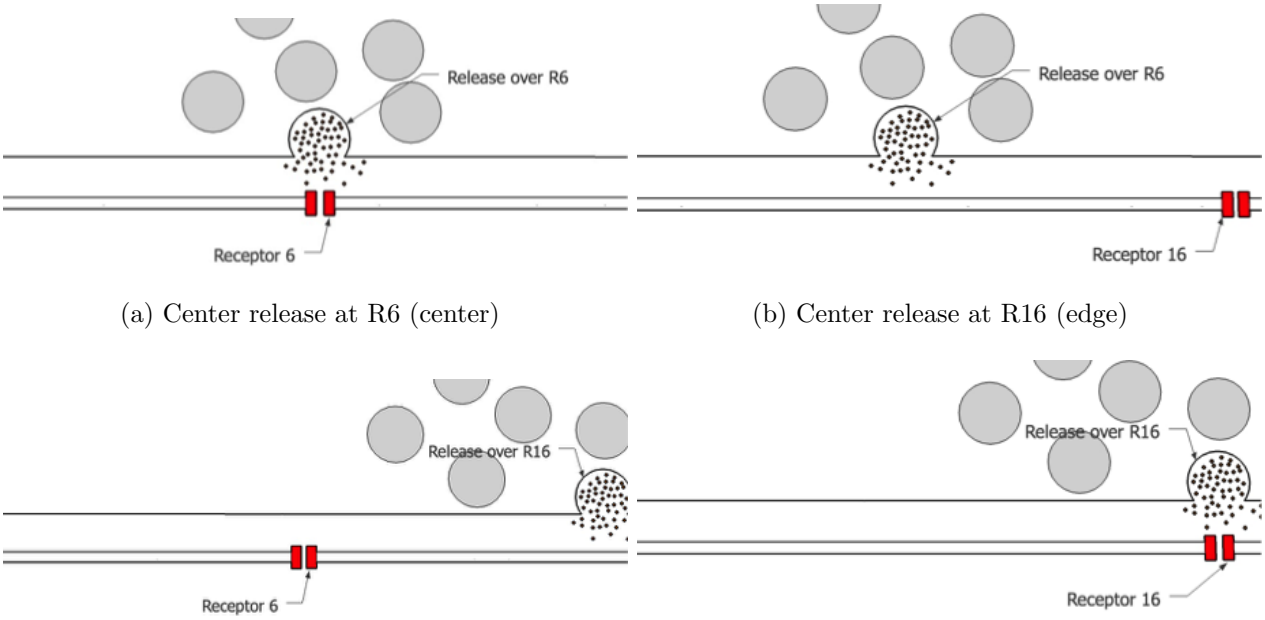

(a) Center release at R6 (center)

(b) Center release at R16 (edge)

(c) Edge release at R6 (center)

(d) Edge release at R16 (edge)

Figure 4.2: Hypothesis of release sites

4.4 Diffusion Model: Support-Operators Model, and Continuous Velocity Model

We use the classical heat diffusion equation in the glutamate release process on the presynaptic terminal. The heat diffusion model is reasonable because of the size of glutamate molecules, and relatively large numbers of the molecules being release as one time. We assume that 4000 glutamate molecules release out from a point source[41]. With an estimated current dose-response profiles obtained from measurements[2, 45], it was widely believed that the glutamate-binding sites become saturated after each synaptic vesicle released[18], and the estimated high glutamate concentration in the cleft after the release of a single synaptic

vesicle is about 1-5mM[10, 12]. This is consistent with simulated values using equation 4.1 with initial concentration of 4,000 molecules. The governing equation is

$$\frac{\partial C}{\partial t} = D_{glut}\left(\frac{\partial^2 C}{\partial^2 x} + \frac{\partial^2 C}{\partial^2 y} + \frac{\partial^2 C}{\partial^2 z}\right), \tag{4.1}$$

where $[G] = C(x, y, z, t)$ is a glutamate concentration as a function of time and location in the vesicular space, the synaptic cleft, and the external space, whereas $t \in [0, \infty)$ and (x, y, z) is in a open region Ω. The coefficient D_{glut} is the thermal diffusivity.

The diffusion coefficients D_{glut} can represent the inhomogeneity of media within the cleft with varying D_{glut}. The larger diffusion coefficient value means for glutamate to flush out to external space quickly. We take D_{glut} in different values depending on the location within or outside the synapse. For a typical synapse, the value of $0.4\mu m^2/ms$ is sufficient to represent typical case of glutamate mobility[41]. However, this may or may not be the case with small synapses, where the evoked and spontaneous releases occur in much closer space. The exact value of D_{glut} is unknown, we used values ranging from 0.1 to $0.75\mu m^2/ms$ as feasible permeability values for synapse. Further we can create multiple zones where D_{glut} could have various values in several zones.

4.4.1 Support-Operators Model

In current mathematical physiology, the classical heat diffusion equation is taken to track of chemical concentrations. A size of vesicle pore containing glutamate molecules is in nano scale, our problem for release process on a single synapse is laid on the border of classical mechanics and quantum mechanics. We first focus on the property of classical mechanics and introduce Support-Operators model. In this model, the number of molecules is infinite. It may or may not be different for velocity of concentrations between two different

materials although flux is continuous across the interface. However, this existing model may or may not perfectly match with our problem because classical mechanics provides accurate results if we consider large objects.

4.4.2 Continuous Velocity Model

We suggest the Continuous Velocity model, a supplementary model adopting both properties of particle dynamics. We assumed that 4000 glutamate molecules diffuse out from a single vesicle pore, and it will take a few moment (approximating $10ms$) to clear out of the cleft. Thus, we assume that velocity is continuous within the time flushing out even if there are different materials in the cleft.

4.5 Kinetics Model in Reaction Diagram on the Postsynaptic Neuron

Under the glutamate mediation, receptors such as NMDA, AMPA or GABA activate the channels for allowing ion currents. To determine the opening probability, P_{open}, of an individual receptor, a state model is proposed based on the maximum likelihood method using experimental data. The current model consisting of three closed and two open states (3C2O) is used by Popescu data[47, 3]. Our calculation will be based on this 3C2O model. We note that the glutamate concentrations at the receptor locations are included in the reaction rates of two coupled states, $C^M$and C^U.

The experimental data indicated the populations of synapses are clustered around 3 groups of distinct characters named as high group, medium group and low group for higher, medium and lower levels of opening probability. We primarily tested our hypotheses on the

medium and low groups as the high group occurs very infrequently. The medium group called M-mode is modeled by

$$C^U \underset{58}{\overset{39[G]}{\rightleftharpoons}} C^M \underset{116}{\overset{19[G]}{\rightleftharpoons}} C_1 \underset{173}{\overset{150}{\rightleftharpoons}} C_2 \underset{2{,}412}{\overset{902}{\rightleftharpoons}} C_3 \underset{1{,}283}{\overset{4{,}467}{\rightleftharpoons}} O_1 \underset{526}{\overset{4{,}630}{\rightleftharpoons}} O_2, \tag{4.2}$$

and the low group(called L-mode kinetics) is modeled as following,

$$C^U \underset{60}{\overset{38[G]}{\rightleftharpoons}} C^M \underset{120}{\overset{17[G]}{\rightleftharpoons}} C_1 \underset{161}{\overset{127}{\rightleftharpoons}} C_2 \underset{2{,}610}{\overset{580}{\rightleftharpoons}} C_3 \underset{2{,}167}{\overset{2{,}508}{\rightleftharpoons}} O_1 \underset{662}{\overset{3{,}449}{\rightleftharpoons}} O_2. \tag{4.3}$$

4.5.1 Systems of ODEs for Kinetic model

We build the ode systems using kinetic model for open probability at each receptor when glutamate molecules releases occur. The open probability is obtained by $P_{open} = O_1(t) + O_2(t)$ [3]. The populations in M-mode and L-mode satisfy the following system of ordinary differential equations respectively.

For M-mode kinetics, we have

$$\begin{aligned}
\frac{dC^U}{dt} &= 58C^M - 39C(x,y,z,t)C^U, \\
\frac{dC^M}{dt} &= (116C_1 - 19C(x,y,z,t)C^M) - (58C^M - 39C(x,y,z,t)C^U), \\
\frac{dC_1}{dt} &= -(116C_1 - 19C(x,y,z,t)C^M) + (173C_2 - 150C_1), \\
\frac{dC_2}{dt} &= (2412C_3 - 902C_2) - (173C_2 - 150C_1), \\
\frac{dC_3}{dt} &= -(2412C_3 - 902C_2) + (1283O_1 - 4467C_3), \\
\frac{dO_1}{dt} &= (526O_2 - 4630O_1) - (1283O_1 - 4467C_3), \\
\frac{dO_2}{dt} &= -(526O_2 - 4630O_1).
\end{aligned}$$

The following system of ordinary differential equations depicts L-mode kinetics:

$$\begin{aligned}
\frac{dC^U}{dt} &= 60C^M - 38C(x,y,z,t)C^U, \\
\frac{dC^M}{dt} &= (120C_1 - 17C(x,y,z,t)C^M) - (60C^M - 38C(x,y,z,t)C^U), \\
\frac{dC_1}{dt} &= -(120C_1 - 17C(x,y,z,t)C^M) + (161C_2 - 127C_1), \\
\frac{dC_2}{dt} &= (2610C_3 - 580C_2) - (161C_2 - 127C_1), \\
\frac{dC_3}{dt} &= -(2610C_3 - 580C_2) + (2167O_1 - 2508C_3), \\
\frac{dO_1}{dt} &= (662O_2 - 3449O_1) - (2167O_1 - 2508C_3), \\
\frac{dO_2}{dt} &= -(662O_2 - 3449O_1).
\end{aligned}$$

4.5.2 Receptor Locations

For the base model (600nm by 600nm cross-section), we assume the NMDA receptor density of 40 per μm^2. On the postsynaptic cleft, there are evenly distributed 16 receptors, arranged in a 4 by 4 array using row-major ordering, as shown in Figure 4.3. The concentration time course and P_{open} are calculated at each receptor. Two representative locations of receptors are used as release sites, R6 for central release and R16 for release at the edge.

4.5.3 Fusion Pore

The release of glutamate vesicle fusion is assumed to be instantaneous in the base model. We also consider a release of the glutamate molecules through a vesicle by addition of two compartments, one vesicle ($40nm \times 40nm \times 40nm$ of a cube) and the other narrow

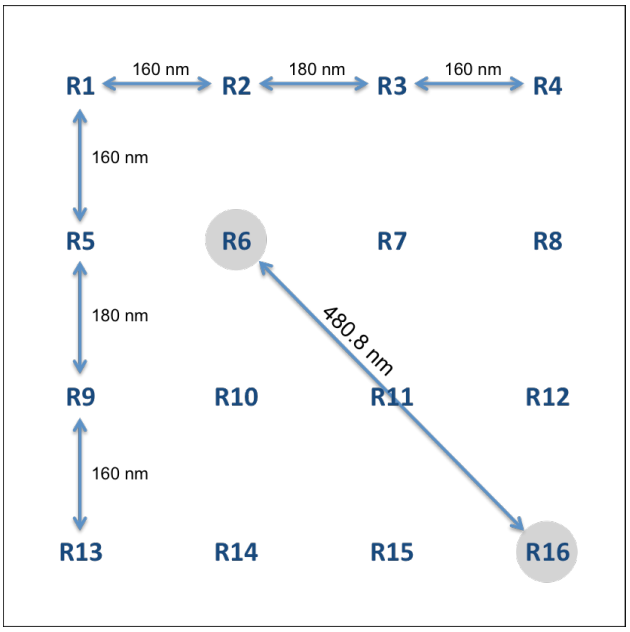

Figure 4.3: Receptor locations for the base model: 16 NMDA receptors are evenly distributed on the postsynaptic terminal surface.

cuboid represented the fusion pore(width of $2nm$ or $10nm$'s) mimicking full fusion or partial fusion events.

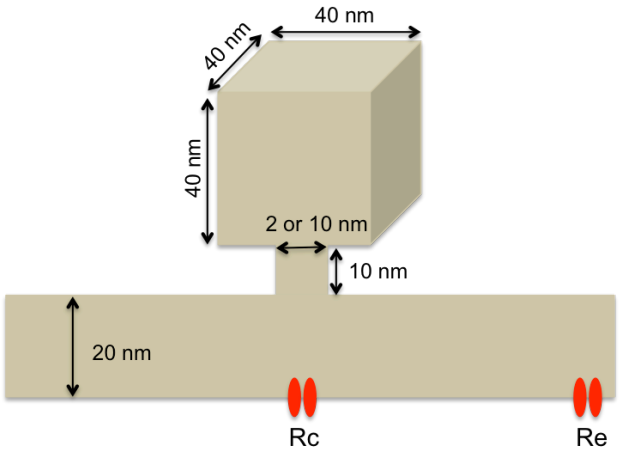

Figure 4.4: Geometry of vesicle fusion pore is consist of a $40 \times 40 \times 40nm^3$ vesicle and a $10 \times 10 \times 10nm^3$ pore. The pore can also be $10 \times 2 \times 2nm^3$ for slower release.

CHAPTER 5

Numerical Methods for Solving Heat Diffusion Equation

5.1 Introduction

In this chapter, we introduce finite difference methods to approximate solutions to heat equations. There are three approaches to be developed, the forward time centered space (FTCS) as an explicit method, the backward time, centered space (BTCS), and Crank-Nicolson schemes, both as an implicit method. The schemes present that how truncation errors depend on mesh spacing and time step. We first show an overview of numerical solutions to the continuous heat equation using finite difference methods, then discuss about the situation with piecewise continuous coefficients.

5.2 The Heat Equation in 1-D

Consider the one-dimensional heat equation,

$$\frac{\partial C}{\partial t} = D\frac{\partial^2 C}{\partial x^2}, \quad t \geq 0, \quad x \in \Omega \tag{5.1}$$

for a region $\Omega \subseteq \mathbb{R}^2$, where the diffusion coefficient D is the diffusivity. In order to obtain the solution from a practical computational, the time should be limited to $t \leq t_{\max} < \infty$. We also need to specify the boundary conditions at $\partial\Omega$. Dirichlet conditions, Neumann

conditions, or mixed conditions can be considered. To keep the presentation as simple and applicable in our problem, only the homogeneous Neumann condition is specified as.

$$\left.\frac{\partial C}{\partial n}\right|_{\partial\Omega} = 0. \tag{5.2}$$

5.3 Finite Difference Approximations in One Variable

The finite difference method is one numerical technique for obtaining approximate solutions to Equation 5.1. The partial differential equation is approximated with the derivatives replaced by the finite difference approximations. We can approximate the derivatives of a known function by finite difference formulas based on values of the function itself at discrete points[29]. From the way, we can solve a large algebraic system of linear equations easily on a computer.

For a mesh $P = \{x_1, x_2, \cdots, x_n\}$ of $\Omega \subseteq \mathbb{R}^1$, denote $C_i = C(x_i)$. The finite difference method involves using discrete approximations like

$$\frac{\partial C}{\partial x} \approx \frac{C_{i+1} - C_i}{\Delta x}. \tag{5.3}$$

The resulting formulas are then used to approximate derivatives with respect to either space or time.

5.3.1 First Order Forward Difference

Consider a Taylor series expansion $C(x)$ about the point x_i

$$C(x_i + \Delta x) = C(x_i) + \Delta x \left.\frac{\partial C}{\partial x}\right|_{x_i} + \frac{(\Delta x)^2}{2!}\left.\frac{\partial^2 C}{\partial x^2}\right|_{\xi}, \; x_i \le \xi \le x_i + \Delta x. \tag{5.4}$$

Solve the Equation 5.4 for $\left.\frac{\partial C}{\partial x}\right|_{x_i}$, we have

$$\left.\frac{\partial C}{\partial x}\right|_{x_i} = \frac{C(x_i + \Delta x) - C(x_i)}{\Delta x} - \left.\frac{\Delta x}{2!}\frac{\partial^2 C}{\partial x^2}\right|_{\xi}. \tag{5.5}$$

Substitute the approximate solution for the exact solution. We use $C_i \approx C(x_i)$ and $C_{i+1} \approx C(x_i + \Delta x)$. Therefore

$$\left.\frac{\partial C}{\partial x}\right|_{x_i} \approx \frac{C_{i+1} - C_i}{\Delta x} - \left.\frac{\Delta x}{2!}\frac{\partial^2 C}{\partial x^2}\right|_{\xi}. \tag{5.6}$$

Or we can rewrite this Expression 5.6 as

$$\left.\frac{\partial C}{\partial x}\right|_{x_i} - \frac{C_{i+1} - C_i}{\Delta x} \approx \left.\frac{\Delta x}{2!}\frac{\partial^2 C}{\partial x^2}\right|_{\xi}. \tag{5.7}$$

From the expression 5.7, the term on the right hand side is called the *truncation error* of the finite difference approximation. Since ξ is unknown, $C(x,t)$ is undefined, and $\partial^2 C/\partial x^2$ cannot be computed, the exact amount of truncation error can not be evaluated. Instead, we use the "big O" notation defined as $\left|\frac{O(\Delta x)}{\Delta x}\right| \leq M$ as $\Delta x \to 0$ for some $M > 0$. In Equation 5.7, the mesh spacing term is Δx, the truncation error can be written as

$$\left.\frac{\Delta x}{2!}\frac{\partial^2 C}{\partial x^2}\right|_{\xi} = O(\Delta x). \tag{5.8}$$

The equality in the Expression 5.8 is not strictly equal, but it shows the order of magnitude sense. Therefore, the first order forward difference formula is

$$\left.\frac{\partial C}{\partial x}\right|_{x_i} = \frac{C_{i+1} - C_i}{\Delta x} + O(\Delta x), \tag{5.9}$$

and its truncation error is $O(\Delta x)$.

5.3.2 First Order Backward Difference

There is an alternative first order finite difference formula that is obtained from the Equation 5.4 replacing Δx with $-\Delta x$. Then we obtain

$$C_{i-1} = C_i - \Delta x \left.\frac{\partial C}{\partial x}\right|_{x_i} + \frac{(\Delta x)^2}{2!}\left.\frac{\partial^2 C}{\partial x^2}\right|_{\xi}, \; x_i - \Delta x \leq \xi \leq x_i. \tag{5.10}$$

Solve the Equation 5.10 for $\left.\frac{\partial C}{\partial x}\right|_{x_i}$

$$\left.\frac{\partial C}{\partial x}\right|_{x_i} = \frac{C_i - C_{i-1}}{\Delta x} + \frac{\Delta x}{2!}\left.\frac{\partial^2 C}{\partial x^2}\right|_{\xi}. \tag{5.11}$$

Therefore, we can also write with big O notation as

$$\left.\frac{\partial C}{\partial x}\right|_{x_i} = \frac{C_i - C_{i-1}}{\Delta x} + O(\Delta x). \tag{5.12}$$

This is called the backward difference formula.

5.3.3 First Order Central Difference

We can also find another approximation with a difference formula with a second order truncation error. As similar to 5.4 and Equation 5.11, write the Taylor series expansions for C_{i+1} and C_{i-1},

$$C_{i+1} = C_i + \Delta x \frac{\partial C}{\partial x}\bigg|_{x_i} + \frac{(\Delta x)^2}{2!}\frac{\partial^2 C}{\partial x^2}\bigg|_{x_i} + \frac{(\Delta x)^3}{3!}\frac{\partial^3 C}{\partial x^3}\bigg|_{x_i} + \cdots, \tag{5.13}$$

$$C_{i-1} = C_i - \Delta x \frac{\partial C}{\partial x}\bigg|_{x_i} + \frac{(\Delta x)^2}{2!}\frac{\partial^2 C}{\partial x^2}\bigg|_{x_i} - \frac{(\Delta x)^3}{3!}\frac{\partial^3 C}{\partial x^3}\bigg|_{x_i} + \cdots. \tag{5.14}$$

Adding Equation 5.14 and Equation 5.13 gives

$$C_{i+1} - C_{i-1} = 2\Delta x \frac{\partial C}{\partial x}\bigg|_{x_i} + \frac{2(\Delta x)^3}{3!}\frac{\partial^3 C}{\partial x^3}\bigg|_{x_i} + \cdots. \tag{5.15}$$

Solve the Equation 5.15 for $\left.\frac{\partial C}{\partial x}\right|_{x_i}$ and it provides

$$\frac{\partial C}{\partial x}\bigg|_{x_i} = \frac{C_{i+1} - C_{i-1}}{2\Delta x} + O(\Delta x^2). \tag{5.16}$$

This is called the central difference approximation.

5.3.4 Second Order Central Difference

Adding Equation 5.14 and Equation 5.13 gives

$$C_{i+1} + C_{i-1} = 2C_i + (\Delta x)^2 \frac{\partial^2 C}{\partial x^2}\bigg|_{x_i} + \frac{2(\Delta x)^4}{4!}\frac{\partial^4 C}{\partial x^4}\bigg|_{x_i} + \cdots, \tag{5.17}$$

Solving for $\left.\frac{\partial^2 C}{\partial x^2}\right|_{x_i}$ yields to

$$\left.\frac{\partial^2 C}{\partial x^2}\right|_{x_i} = \frac{C_{i+1} - 2C_i + C_{i+1}}{\Delta x^2} + O(\Delta x^2). \tag{5.18}$$

5.4 Explicit Scheme for Heat Equation

We can develop now the finite difference approximations for Heat Equation. Both the time and space derivatives are replaced by finite differences. In this case, we will have one subscript n to designate the time step. The finite difference model can be implemented by a software such as MATLAB.

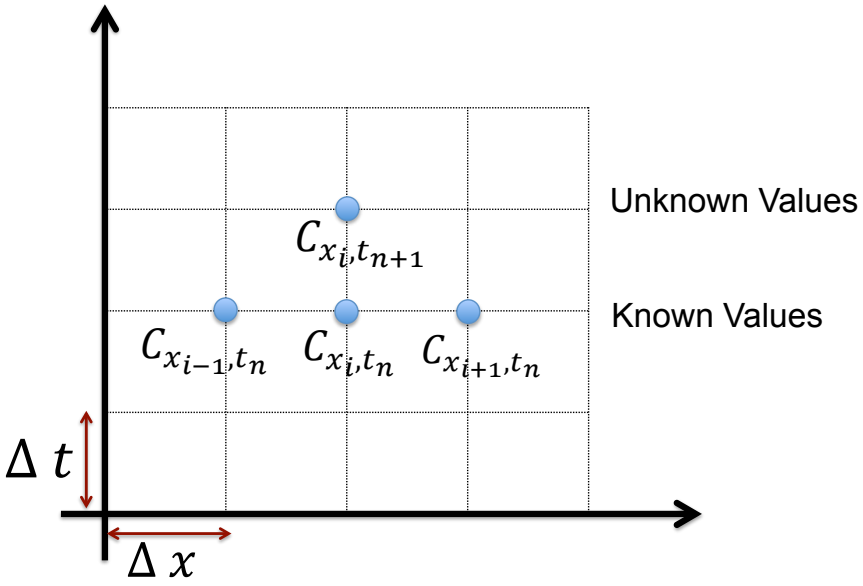

Figure 5.1: A formula for the unknown 'Concentration' $C_{i,t+1}$ at the $(t+1)$-th time in terms of known 'Concentration' along the t-th time row.

5.4.1 Forward Time, Centered Space (FTCS)

First, we approximate the time derivative in Equation 5.1 with a forward difference,

$$C(x_i, t_n + \Delta t) = C(x_i, t_n) + \Delta t \left.\frac{\partial C}{\partial t}\right|_{(x_i,t_n)} + \frac{(\Delta t)^2}{2!} \left.\frac{\partial^2 C}{\partial t^2}\right|_{(x_i,t_n)} + \cdots . \tag{5.19}$$

Then solving Equation 5.19 for $\left.\frac{\partial C}{\partial t}\right|_{(x_i,t_n)}$ leads to

$$\left.\frac{\partial C}{\partial t}\right|_{(x_i,t_n)} = \frac{C(x_i, t_n + \Delta t) - C(x_i, t_n)}{\Delta t} - \frac{\Delta t}{2!} \left.\frac{\partial^2 C}{\partial t^2}\right|_{(x_i,t_n)} - \cdots . \tag{5.20}$$

Denote $t_{n+1} = t_n + \Delta t$. Substitute the approximate solution for the exact solution, we use $C_i^n \approx C(x_i, t_n)$ and $C_i^{n+1} \approx C(x_i, t_{n+1}) = C(x_i, t_n + \Delta t)$. Using big O notation, then we get

$$\left.\frac{\partial C}{\partial t}\right|_{(x_i,t_n)} = \frac{C_i^{n+1} - C_i^n}{\Delta t} + O(\Delta t). \tag{5.21}$$

Next, we obtain $\left.\frac{\partial^2 C}{\partial x^2}\right|_{(x_i,t_n)}$ which appears on the right hand side of Equation 5.1, and evaluate all terms at time t_n.

$$\left.\frac{\partial^2 C}{\partial x^2}\right|_{(x_i,t_n)} = \frac{C_{i-1}^n - 2C_i^n + C_{i+1}^n}{\Delta x^2} + O(\Delta x^2). \tag{5.22}$$

Substituting Equation 5.21 and Equation 5.22 in Equation 5.1, we get

$$\frac{C_i^{n+1} - C_i^n}{\Delta t} = D\frac{C_{i-1}^n - 2C_i^n + C_{i+1}^n}{\Delta x^2} + O(\Delta t) + O(\Delta x^2). \tag{5.23}$$

Solving explicitly for C_i^{n+1} in terms of the other values of C yields

$$C_i^{n+1} = C_i^n + \frac{D\Delta t}{\Delta x^2}(C_{i+1}^n - 2C_i^n + C_{i-1}^n) \tag{5.24}$$

The equation 5.24 is called Forward Time, Centered Space or FTCS approximation to the heat equation. The FTCS can have unstable solutions if Δt is too large. Therefore, we can obtain stable solutions when $\alpha = \frac{D\Delta t}{\Delta x^2} < \frac{1}{2}$ for CFL condition[31].

5.5 Implicit Scheme for Heat Equation

5.5.1 Backward Time, Centered Space (BTCS)

We use the backward difference to approximate the time derivative,

$$\left.\frac{\partial C}{\partial t}\right|_{(x_i,t_n)} = \frac{C_i^n - C_i^{n-1}}{\Delta t} + O(\Delta t). \tag{5.25}$$

Then we have BTCS scheme for Heat Equation as following :

$$\frac{C_i^n - C_i^{n-1}}{\Delta t} = D\frac{C_{i-1}^n - 2C_i^n + C_{i+1}^n}{\Delta x^2} + O(\Delta t) + O(\Delta x^2). \tag{5.26}$$

An advantage for solutions to the heat equation by BTCS scheme is unconditionally stable, however, it has a higher computational cost at each time step[1, 48].

5.5.2 Crank-Nicolson Scheme

The Crank-Nicolson scheme has a temporal truncation error $O(\Delta t^2)$, which compares to that of FTCS and BTCS, $O(\Delta t)$. The heat equation is approximated to

$$\frac{C_i^n - C_i^{n-1}}{\Delta t} = \frac{D}{2}\left[\frac{C_{i-1}^n - 2C_i^n + C_{i+1}^n}{\Delta x^2} + \frac{C_{i-1}^{n-1} - 2C_i^{n-1} + C_{i+1}^{n-1}}{\Delta x^2}\right]. \tag{5.27}$$

The Crank-Nicolson scheme is implicit scheme that requires solving a system of equations at each time step. However, the truncation error is $O(\Delta t^2)+O(\Delta x^2)$ and this is smaller than the truncation error of the FTCS and BTCS schemes. The scheme is numerically implemented in the our neuroscience problems.

5.6 Discontinuous Diffusion Coefficients

Several finite difference methods for solving the piecewise continuous heat equations in three dimensional space have been seen in the literature. In 1999, Li and Shen provided a finite difference method which allows to a different coefficient value for each sub-region of interfaces in 2D and proved its second order accuracy[34]. We proposed this numerical method in three dimensional space for a cubic domain, and prove its second order accuracy. We further applied this method to a diffusion process for Glutamate release in a synapse, and validated the method for second order accuracy numerically.

The heat diffusion equation,

$$\frac{\partial C}{\partial t} = \nabla \cdot (D\nabla C), \quad t \geq 0, \quad (x, y, z) \in \Omega, \tag{5.28}$$

in a cubic shaped domain $\Omega = (a, b) \times (a, b) \times (c, d)$ in $\mathbb{R}^3$. Within the region, suppose diffusion coefficient D is piecewise continuous. Heat diffusion with discontinuous coefficients

arises when heat transfer occurs at an interface of two different materials. In our neuroscience problems, we will use the model for glutamate diffusion in synapse clefts. We define two sub-regions Ω^+, Ω^- separated by an interface Γ. We assume homegeneous Neumann boundary conditions

$$\left.\frac{\partial C}{\partial n}\right|_{\partial\Omega} = 0. \tag{5.29}$$

Define $\Omega^+ = \{(a_1, b_1) \times (a_1, b_1) \times (c, d)\}$, with $a < a_1 < b_1 < b$, and $\Omega^- = \Omega \setminus \Omega^+$.

Let D be a piecewise constant function in Ω as

$$D(x, y, z) = \begin{cases} D^+, & (x, y, z) \in \Omega^+, \\ D^-, & (x, y, z) \in \Omega^-. \end{cases}$$

Assume that the initial condition at $t = 0$ is smooth and the boundary conditions on $\partial\Omega$ are known, the solution is uniquely determined in $W^{1,1}(\Omega)$ [6].

The theory for interfaces implies that the concentration C is continuous across the interfaces Γ, and the normal flux is continuous across the interface Γ [32, 55]. Considering the condition, we have

$$[C] = 0, \tag{5.30}$$

$$[DC_n] = 0. \tag{5.31}$$

But the tangential flux may or may not be continuous across Γ.

5.6.1 Model 1: The Support-Operators Method (Harmonic-Averaging)

An approach for the numerical solution of the heat diffusion solution in heterogeneous media is derived using the support-operator method, which constructs discrete analogs of

divergence and flux operator [55]. For regular grids, the discrete operators for discontinuous diffusion coefficients are equivalent to the harmonic-averaging procedure. Also the scheme is second-order accurate.

First, we look at the flux vector $\mathbf{J}$ whose form of diffusion equation is commonly used in the case of discontinuous D. The heat diffusion equation 5.28 can be written as a first-order system:

$$\frac{\partial C}{\partial t} = -\nabla \mathbf{J}, \quad \mathbf{J} = -D\nabla u. \tag{5.32}$$

The heat diffusion equation is semi-discretized implicitly as following:

$$\frac{C^{n+1} - C^n}{\Delta t} = \nabla \cdot D\nabla C^{n+1} \tag{5.33}$$

where $t_n = n\Delta t$ and $C^n = C(t_n, x, y, z)$.

The flux form of the equation 5.32 can be discretized in time as following.

$$\mathbf{J}^{n+1} = -D\nabla C^{n+1}, \quad \frac{(C^{n+1} - C^n)}{\Delta t} + \nabla \cdot \mathbf{J}^{n+1} = 0. \tag{5.34}$$

The discretization of support-operators for the diffusion coefficients D at rectangular grids leads to the harmonic average. To induce the discrete analog of $\nabla \cdot D\nabla C$, we denote the diffusion coefficients on the interfaces using harmonic averaging,

$$D\xi_{(i,j,k)} = \frac{2D_{(i-1,j,k)}D_{(i,j,k)}}{D_{(i-1,j,k)} + D_{(i,j,k)}},$$

$$D\eta_{(i,j,k)} = \frac{2D_{(i,j-1,k)}D_{(i,j,k)}}{D_{(i,j-1,k)} + D_{(i,j,k)}},$$

$$D\zeta_{(i,j,k)} = \frac{2D_{(i,j,k-1)}D_{((i,j,k)}}{D_{(i,j,k-1)} + D_{(i,j,k)}}.$$

Denote $C = C(x_i, y_j, z_k, t_n) \equiv C_{(i,j,k)}(t)$. The discrete analog of $\nabla \cdot D\nabla C$ is as following:

$$\frac{D\xi_{(i+1,j,k)}\frac{C_{(i+1,j,k)}-C_{(i,j,k)}}{\Delta x} - D\xi_{(i,j,k)}\frac{C_{(i,j,k)}-C_{(i-1,j,k)}}{\Delta x}}{\Delta x}$$

$$+\frac{D\eta_{(i,j+1,k)}\frac{C_{(i,j+1,k)}-C_{(i,j,k)}}{\Delta y} - D\eta_{(i,j,k)}\frac{C_{(i,j,k)}-C_{(i,j-1,k)}}{\Delta y}}{\Delta y}$$

$$+\frac{D\zeta_{(i,j,k+1)}\frac{C_{(i,j,k+1)}-C_{(i,j,k)}}{\Delta z} - D\zeta_{(i,j,k)}\frac{C_{(i,j,k)}-C_{(i,j,k-1)}}{\Delta z}}{\Delta z}.$$

The scheme is second-order accurate in truncation errors for the numerical solution of diffusion problems in heterogeneous and nonisotropic materials constructed in rectangular grids[55].

In this model, the number of molecules is assumed to be infinite. It may or may not be a difference for velocity of concentrations between two different materials. However, this existing model may or may not perfectly match with our problem because the number of molecules is limited in our study.

5.6.2 Model 2: Continuous Velocity Model

In our problem, 4000 glutamate molecules diffuse out from a single vesicle pore, and it will take a few moments (approximating $10ms$) to clear out of the cleft. The particle velocity may also be continuous within the time flushing out even if there are different materials in the cleft. We assume the derivative is continuous at Γ to reflect the scenario of fewer particles moving in a porous medium. Because the velocity is continuous on the interface, there is no jump of the first derivative in normal direction. Thus, we do not treat a point on the interface as a grid point, but is located in between two grids points(see in Figure 5.2).

Given a new structured mesh in a cubic domain, we classify all grid points in Ω into two sets. The set P_{reg} consists "regular points", any point in one sub-region Ω^+ or Ω^- that has no neighbor point in the other sub-region. The set P_{irr} contains "irregular points", any point in one sub-region Ω^+ or Ω^- that has at least one neighbor point in the other sub-region.

First, we discretize the solution in the x-direction, y-direction, and z-direction with a mesh of size h. Let $C_{i,j,k}$ be a numerical solution,

$$C_{xx} \approx \frac{1}{h^2}(C_{i-1,j,k} - 2C_{i,j,k} + C_{i+1,j,k}) \equiv \delta_x C_{i,j,k}, \tag{5.35}$$

$$C_{yy} \approx \frac{1}{h^2}(C_{i,j-1,k} - 2C_{i,j,k} + C_{i,j+1,k}) \equiv \delta_y C_{i,j,k}, \tag{5.36}$$

$$C_{zz} \approx \frac{1}{h^2}(C_{i,j,k-1} - 2C_{i,j,k} + C_{i,j,k+1}) \equiv \delta_z C_{i,j,k}. \tag{5.37}$$

5.6.3 Regular Grid Point

For a regular grid point (x, y, z), assume the exact solution $C(x, y, z)$ is smooth then by Taylor expansions, $\delta_x C_{i,j,k}$ can be denoted by

$$\delta_x C_{i,j,k} = \left[C_{xx}(x_i, y_j, z_k) + \frac{1}{12}h^2 C^{(4)}(x_i, y_j, z_k) + O(h^4)\right] \tag{5.38}$$

Therefore,

$$\tau_x = C_{xx} - \delta_x C_{i,j,k} = -\frac{1}{12}h^2 C^{(4)}(x_i, y_j, z_k) + O(h^4). \tag{5.39}$$

Also $C_{yy} - \delta_y C_{i,j,k}$, $C_{zz} - \delta_z C_{i,j,k}$ are similar. The local truncation error of 5.35, 5.36, and 5.37 from $(DC_x)_x + (DC_y)_y + (DC_z)_z$ is $O(h^2)$.

5.6.4 Irregular Grid Point

For an irregular grid point (x, y, z), we need additional correction terms in Equations 5.35, 5.36, and 5.37 and we prove the local truncation error is $O(h)$.

In this paper, the interface $\Gamma = \partial\Omega^+$ is cubic shape and Γ consists of all points on surfaces, edges, and corners of a cubic domain. Now we denote

$$\Gamma = S \cup E \cup C$$

where S is the set of all points on surfaces, E is the set of all points on edges, and C is the set of all points on corners of Γ.

Let $[C]$ denote the difference of the limits of C cross the discontinuity from exterior(Ω^+) to interior(Ω^-) along the normal direction.

$$[C] \equiv C^+ - C^- = 0, \tag{5.40}$$

$$[C_n] \equiv C_n^+ - C_n^- = 0. \tag{5.41}$$

Equation 5.41 is a modeling constraint of interface, assuming no change of normal velocity across the interface.

First, let (x_i, y_j, z_k) an irregular grid point adjacent to a surface($S \subset \Gamma$). Without loss of generality, we assume S is parallel to (y, z)-plane.

Then from Equation 5.28

$$[C_{xx}] = \left[\frac{C_t}{D}\right], \text{and } [C_{yy}] = [C_{zz}] = 0 \tag{5.42}$$

because there is no jump in y, z direction and $C(x, y, z, t)$ is continuous across Γ. Now we consider the 2nd derivative jump in x-direction. There are four cases to discuss:

(a) $(x_i, y_j, z_k) \in \Omega^+$, $(x_{i+1}, y_j, z_k) \in \Omega^-$,

(b) $(x_i, y_j, z_k) \in \Omega^-$, $(x_{i-1}, y_j, z_k) \in \Omega^+$,

(c) $(x_i, y_j, z_k) \in \Omega^-$, $(x_{i+1}, y_j, z_k) \in \Omega^+$,

(d) $(x_i, y_j, z_k) \in \Omega^+$, $(x_{i-1}, y_j, z_k) \in \Omega^-$.

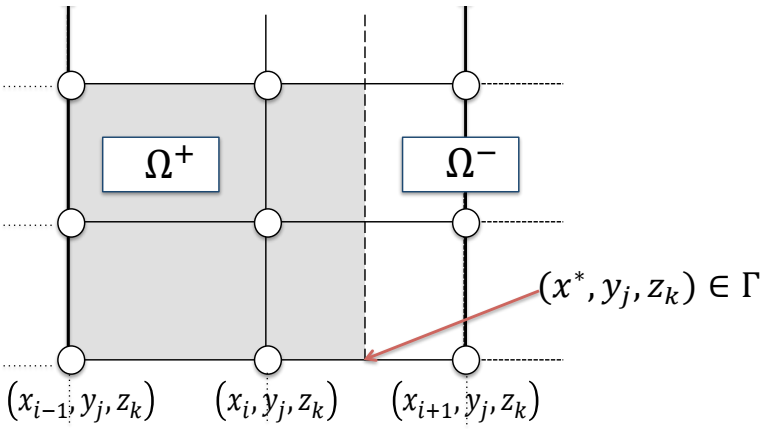

Figure 5.2: Mesh points used for solving the three dimensional heat equation. The grey area indicates Ω^+, and the white area indicates Ω^-.

For case (a), let the intersection point of the line segment connecting (x_i, y_j, z_k), (x_{i+1}, y_j, z_k) and Γ be (x^*, y_j, z_k). Using Taylor's series around x^*, we have

$$\begin{aligned}
&\frac{1}{h^2}(C(x_{i-1}, y_j, z_k) - 2C(x_i, y_j, z_k) + C(x_{i+1}, y_j, z_k)) \\
&= \frac{1}{h^2}\{[C] + [C_x](x_{i+1} - x^*) + \frac{[C_{xx}]}{2!}(x_{i+1} - x^*)^2\} + C^-_{xx} + O(h) \\
&= \frac{1}{h^2}\{\frac{[C_{xx}]}{2!}(x_{i+1} - x^*)^2\} + C^-_{xx} + O(h)
\end{aligned}$$

since $[C] = [C_x] = 0$ across Γ from our model assumption.

This implies

$$C_{xx} = \delta_x C_{i,j,k} - \frac{\left[\frac{C_t}{D}\right](x_{i+1} - x^*)^2}{2h^2} + O(h). \tag{5.43}$$

Similarly, for case (b), we drive

$$C_{xx} = \delta_x C_{i,j,k} + \frac{\left[\frac{C_t}{D}\right](x_{i-1} - x^*)^2}{2h^2} + O(h). \tag{5.44}$$

For case (c), we get

$$C_{xx} = \delta_x C_{i,j,k} + \frac{\left[\frac{C_t}{D}\right](x_{i+1} - x^*)^2}{2h^2} + O(h). \tag{5.45}$$

For case (d), we have

$$C_{xx} = \delta_x C_{i,j,k} - \frac{\left[\frac{C_t}{D}\right](x_{i-1} - x^*)^2}{2h^2} + O(h) \tag{5.46}$$

Analogously, the point is an irregular point near a surface in the y-direction and z-direction, we have similar estimates. We add correction terms such that the local truncation is $O(h)$.

Now, consider (x_i, y_j, z_k) be an irregular point adjacent to an edge ($E \subset \Gamma$). Assume without loss of generality, E is parallel to z-axis at the intersection of x-plane and y-plane. Then we have

$$[C_{xx}] = [C_{yy}] = \left[\frac{C_t}{D}\right], \text{and } [C_{zz}] = 0. \tag{5.47}$$

Using correction terms in both x-direction, y-direction due to discontinuity, we obtain a system of ordinary differential equations:

$$\begin{aligned}(C_{i,j,k})_t =& D(\delta_x C_{i,j,k} + \delta_y C_{i,j,k} + \delta_z C_{i,j,k}) \\ &+ D\left[\frac{C_t}{D}\right]\frac{\tau_{x_0}(x_{i_0} - x^*)^2}{2h^2} + D\left[\frac{C_t}{D}\right]\frac{\tau_{y_0}(y_{j_0} - y^*)^2}{2h^2} + O(h)\end{aligned}$$

where $i_0 = i - 1$ or $i + 1$, $j_0 = j - 1$ or $j + 1$. $\tau_{x_0}, \tau_{y_0} = 1$ or -1.

Similarly, for (x_i, y_j, z_k) be an irregular point adjacent to x, z-edge ($E \subset \Gamma$), we have

$$\begin{aligned}(C_{i,j,k})_t =& D(\delta_x C_{i,j,k} + \delta_y C_{i,j,k} + \delta_z C_{i,j,k}) \\ &+ D\left[\frac{C_t}{D}\right]\frac{\tau_{x_0}(x_{i_0} - x^*)^2}{2h^2} + D\left[\frac{C_t}{D}\right]\frac{\tau_{z_0}(z_{k_0} - z^*)^2}{2h^2} + O(h),\end{aligned}$$

where $i_0 = i - 1$ or $i + 1$, $k_0 = k - 1$ or $k + 1$. $\tau_{x_0}, \tau_{z_0} = 1$ or -1.

For (x_i, y_j, z_k) be an irregular point adjacent to y, z-edge ($E \subset \Gamma$), we obtain

$$\begin{aligned}(C_{i,j,k})_t =& D(\delta_x C_{i,j,k} + \delta_y C_{i,j,k} + \delta_z C_{i,j,k}) \\ &+ D\left[\frac{C_t}{D}\right]\frac{\tau_{y_0}(y_{j_0} - y^*)^2}{2h^2} + D\left[\frac{C_t}{D}\right]\frac{\tau_{z_0}(z_{k_0} - z^*)^2}{2h^2} + O(h)\end{aligned}$$

where $j_0 = j - 1$ or $j + 1$ and $k_0 = k - 1$ or $k + 1$. $\tau_{y_0}, \tau_{z_0} = 1$ or -1.

Finally, let (x_i, y_j, z_k) be an irregular point adjacent to a corner ($C \subset \Gamma$). Then we use similar analysis to obtain

$$[C_{xx}] = [C_{yy}] = [C_{zz}] = \left[\frac{C_t}{D}\right]. \tag{5.48}$$

We use correction terms in three directions, x-direction, y-direction, and z-direction. Let (x^*, y^*, z^*) be the actual corner, then we have

$$\begin{aligned}(C_{i,j,k})_t =& D(\delta_x C_{i,j,k} + \delta_y C_{i,j,k} + \delta_z C_{i,j,k}) \\ &+ D\left[\frac{C_t}{D}\right]\frac{\tau_{x_0}(x_{i_0} - x^*)^2}{2h^2} + D\left[\frac{C_t}{D}\right]\frac{\tau_{y_0}(y_{j_0} - y^*)^2}{2h^2} + D\left[\frac{C_t}{D}\right]\frac{\tau_{z_0}(z_{k_0} - z^*)^2}{2h^2} + O(h)\end{aligned}$$

where $i_0 = i-1$ or $i+1$, $j_0 = j-1$ or $j+1$, $k_0 = k-1$ or $k+1$, and τ_{x_0}, τ_{y_0}, $\tau_{z_0} = 1$ or -1. Now, we have

$$\left[\frac{C_t}{D}\right] = C_t^- \left[\frac{1}{D}\right] + \frac{[C_t]}{D^+} = C_t^+ \left[\frac{1}{D}\right] + \frac{[C_t]}{D^-}.$$

This implies

$$\left[\frac{C_t}{D}\right] = C_t \left[\frac{1}{D}\right] + \frac{[C_t]}{\widetilde{D}} + O(h). \tag{5.49}$$

where $\widetilde{D} = D^-$ if $D = D^+$, $\widetilde{D} = D^+$ if $D = D^-$. Using 5.49, we have the following system of ordinary differential equations

$$(C_{i,j,k})_t = F(C_{i-1,j,k}, C_{i,j-1,k}, C_{i,j,k-1}, C_{i,j,k}, C_{i+1,j,k}, C_{i,j+1,k}, C_{i,j,k+1}),$$

where F is equal to

$$\frac{D(\delta_x C_{i,j,k} + \delta_y C_{i,j,k} + \delta_z C_{i,j,k} + \frac{[C_t]}{\widetilde{D}}\ T_{i,j,k})}{1 - D[\frac{1}{D}]\ T_{i,j,k}} \tag{5.50}$$

where

$$T_{i,j,k} = \frac{\tau_{x_0}(x_{i_0} - x^*)^2}{2h^2} + \frac{\tau_{y_0}(y_{j_0} - y^*)^2}{2h^2} + \frac{\tau_{z_0}(z_{k_0} - z^*)^2}{2h^2}. \tag{5.51}$$

Finally, we discretize time t by choosing $\Delta t = A \cdot h^2$ for CFL condition where A is a constant[8]. We use explicit Finite Difference method,

$$C^{n+1}_{i,j,k} = C^n_{i,j,k} + \Delta t \cdot F(C^n_{i-1,j,k}, C^n_{i,j-1,k}, C^n_{i,j,k-1}, C^n_{i,j,k}, C^n_{i+1,j,k}, C^n_{i,j+1,k}, C^n_{i,j,k+1})$$

which implies the local truncation error for discretizing on t is $O(\Delta t)$.

5.6.5 Accuracy Analysis

We show that $1 - D[\frac{1}{D}]\ T_{i,j,k}$, which is the denominator of the right-side of Equation 5.50 is bounded below by a positive constant.

Denote :

$$U_{i,j,k} \equiv 1 - D\left[\frac{1}{D}\right]\ T_{i,j,k}, \quad L_{i,j,k} \equiv 1 + \left|D\left[\frac{1}{D}\right]\ T_{i,j,k}\right|.$$

Lemma 5.6.1. *Let $U_{i,j,k}$ and $L_{i,j,k}$ be as defined above. Then*

$$U_{i,j,k} \geq 1, \ \textit{and} \ \ L_{i,j,k} \leq 1 + 3 \cdot max\ (D^+, D^-)\left|\left[\frac{1}{D}\right]\right| \tag{5.52}$$

Proof: We gave a lower bound of $U_{i,j,k}$. In x-direction, we have four cases:

(a) $(x_i, y_j, z_k) \in \Omega^+, (x_{i+1}, y_j, z_k) \in \Omega^-$. Then $x_{i_0} = x_{i+1}, \tau_{x_{i_0}} = 1, D = D^+,$ and $D\left[\frac{1}{D}\right]\tau_{x_{i_0}} = 1 - \frac{D^+}{D^-}$.

(b) $(x_i, y_j, z_k) \in \Omega^+, (x_{i-1}, y_j, z_k) \in \Omega^-$. Then $x_{i_0} = x_{i-1}, \tau_{x_{i_0}} = -1, D = D^-,$ and $D\left[\frac{1}{D}\right]\tau_{x_{i_0}} = 1 - \frac{D^+}{D^-}$.

(c) $(x_i, y_j, z_k) \in \Omega^-, (x_{i+1}, y_j, z_k) \in \Omega^+$. Then $x_{i_0} = x_{i+1}, \tau_{x_{i_0}} = -1, D = D^-,$ and $D\left[\frac{1}{D}\right]\tau_{x_{i_0}} = 1 - \frac{D^-}{D^+}$.

(d) $(x_i, y_j, z_k) \in \Omega^+, (x_{i-1}, y_j, z_k) \in \Omega^-$. Then $x_{i_0} = x_{i-1}, \tau_{x_{i_0}} = 1, D = D^+,$ and $D\left[\frac{1}{D}\right]\tau_{x_{i_0}} = 1 - \frac{D^-}{D^+}$.

For all cases, $D\left[\frac{1}{D}\right]\tau_{x_{i_0}}$ is equal to $1 - \frac{\max\{D^+, D^-\}}{\min\{D^+, D^-\}}$, if $D = \min\{D^+, D^-\}$. Only positive terms will reduce the lower bound of $U_{i,j,k}$. Since $\frac{\max\{D^+, D^-\}}{\min\{D^+, D^-\}} > 1$, then

$$U_{i,j,k} \geq 1 - \left\{1 - \frac{\max\,(D^+, D^-)}{\min\,(D^+, D^-)}\right\} - \left\{1 - \frac{\max(D^+, D^-)}{\min(D^+, D^-)}\right\} - \left\{1 - \frac{\max(D^+, D^-)}{\min(D^+, D^-)}\right\} \geq 1$$

We can also provide an upper bound of $L_{i,j,k}$

$$L_{i,j,k} \leq 1 + D\left|\left[\frac{1}{D}\right]\right| + D\left|\left[\frac{1}{D}\right]\right| + D\left|\left[\frac{1}{D}\right]\right| \leq 1 + 3 \cdot \max(D^+, D^-)\left|\left[\frac{1}{D}\right]\right|$$

Now we have the following theorem.

Theorem 5.6.2. *Let F be defined as in Equation 5.50. At any irregular grid point (x_i, y_j, z_k) in Ω,*

$$F(C_{i-1,j,k}, C_{i,j-1,k}, C_{i,j,k-1}, C_{i,j,k}, C_{i+1,j,k}, C_{i,j+1,k}, C_{i,j,k+1})$$
$$-[(DC_x)_x + (DC_y)_y + (DC_z)_z](x_i, y_j, z_k) = O(h).$$

Proof: From 5.50, we have

$$
\begin{aligned}
F \quad & (C_{i-1,j,k}, C_{i,j-1,k}, C_{i,j,k-1}, C_{i,j,k}, C_{i+1,j,k}, C_{i,j+1,k}, C_{i,j,k+1}) = (C_{i,j,k})_t \\
= \quad & D(\delta_x C_{i,j,k} + \delta_y C_{i,j,k} + \delta_z C_{i,j,k}) \\
& + \left\{ D\left[\frac{1}{D}\right] \frac{\tau_{x_0}(x_{i_0} - x^*)^2}{2h^2} + D\left[\frac{1}{D}\right] \frac{\tau_{y_0}(y_{j_0} - x^*)^2}{2h^2} + D\left[\frac{1}{D}\right] \frac{\tau_{z_0}(z_{k_0} - z^*)^2}{2h^2} \right\} \\
= \quad & D(\delta_x C_{i,j,k} + \delta_y C_{i,j,k} + \delta_z C_{i,j,k}) \\
& + D\left[\frac{C_t}{D}\right] \frac{\tau_{x_0}(x_{i_0} - x^*)^2}{2h^2} + D\left[\frac{C_t}{D}\right] \frac{\tau_{y_0}(y_{i_0} - y^*)^2}{2h^2} + D\left[\frac{C_t}{D}\right] \frac{\tau_{z_0}(z_{k_0} - z^*)^2}{2h^2} + O(h) \\
= \quad & (DC_{xx} + DC_{yy} + DC_{zz})(x_i, y_j, z_k) + O(h)
\end{aligned}
$$

as desired.

Since the interface is one dimension lower than the solution domain, we will need the local truncation error at irregular grid points to be $O(h)$ to obtain second order accuracy globally because interface is two dimensions which is lower than the solution domain, the number of irregular points will be $O(n^2)$ compared to the total number of grid points, $O(n^3)$. Thus, it is enough for the difference scheme at irregular points to be $O(h)$ without affecting second order accuracy globally[33, 34]. At a regular grid point, we achieve the local truncation error is $O(h^2)$. At an irregular grid point, the local truncation error is $O(h)$ by Theorem 5.6.2. The local truncation error from the discretization of time is $O(\Delta t) = O(h^2)$. All these imply that the numerical solution has global error $O(h^2)$.

CHAPTER 6

Simulations for Diffusion Process of Glutamate Release

6.1 Introduction

In this chapter, we simulate the process of glutamate release from presynaptic sites into the synaptic cleft. We obtain the total concentration of released glutamate with the limited time, and the glutamate concentration at each receptor. We used the problem-solving environment MATLAB, which provide tools for solving linear systems in a numerical way. MATLAB is efficient to display results visually through graph in its post-processing.

6.2 MATLAB Implementation

In order to solve the heat equation numerically to achieve glutamate concentration, we use on explicit difference method (forward time, centered space) that is implemented in MATLAB codes.

$$\begin{aligned} C_{i,j,k}^{n+1} &= C_{i,j,k}^{n} + \alpha[S_{i+1,j,k}C_{i+1,j,k}^{n} + S_{i-1j,k}C_{i-1j,k}^{n} + S_{i,j+1,k}C_{i,j+1,k}^{n} + S_{i,j-1,k}C_{i,j-1,k}^{n} \\ &+ S_{i,j,k-1}C_{i,k,j,k-1}^{n} - (S_{i,j,k}C_{i,j,k}^{n} + S_{i-1,j,k}C_{i,j,k}^{n} + S_{i,j+1,k}C_{i,j,k}^{n} + S_{i,j-1,k}C_{i,j,k}^{n} \\ &+ S_{i,j,k+1}C_{i,j,k}^{n} + S_{i,j,k-1}C_{i,j,k}^{n})], \end{aligned}$$

where $C_{i,j,k}^{n} = C(x_i, y_j, z_k, t_n)$ and $\alpha = D_{glut}\dfrac{\Delta t}{(\Delta x)^2}$. For our simulation, we satisfy a condition of $\alpha < (1/2)^3$ known as CFL condition to ensure the scheme is numerically stable[31]. We take the space step $\Delta x = 0.01\mu m$ and the time step $\Delta t = C \cdot (\Delta x)^2$, where C is a constant.

Although the glutamate diffusion coefficients are not measured directly, we use those values from 0.1 to $0.7\mu m^2/ms$. Whereas, the diffusion constant is larger, it indicates that neurotransmitters flush out quickly, in other words, there are less barriers for glutamates to move away from the release sites. Independent signaling of two transmissions is influenced by the time duration of glutamate diffusion.

We take various diffusion coefficients D_{glut} depending on the location within or outside the synapses. In base model, we have a value of $D_{glut} = 0.4\mu m^2/ms$ within the cleft and $D_{glut} = 0.75\mu m^2/ms$ in the external space. When simulating the vesicular diffusion, $D_{glut} = 0.15\mu m^2/ms$ and $D_{glut} = 0.0375\mu m^2/ms$ are taken for 10nm and 2nm fusion pore respectively.

6.3 Main Results

As shown in Figure 4.2, we assume the situation where evoked glutamate release activates evoked receptor kinetics at center and spontaneous receptor kinetics at edge. Spontaneous glutamate release at the cleft edge activates evoked receptor kinetics at center and spontaneous receptor kinetics at edge.

First, we simulate the base model with an instantaneous release of 4000 glutamate molecules. Figure 6.1 shows the total number of molecules within the cleft decreases according to the time when center release and edge release occur. It takes about 0.08ms to clear a half of the molecules out of the cleft and the population decays in exponential trends with decay constants 8.808×10^{-5} and 4.526×10^{-4} respectively, as shown Figure 6.1a and 6.1b. It implies that a edge release makes glutamate molecules flushed out much quicker than that of center release.

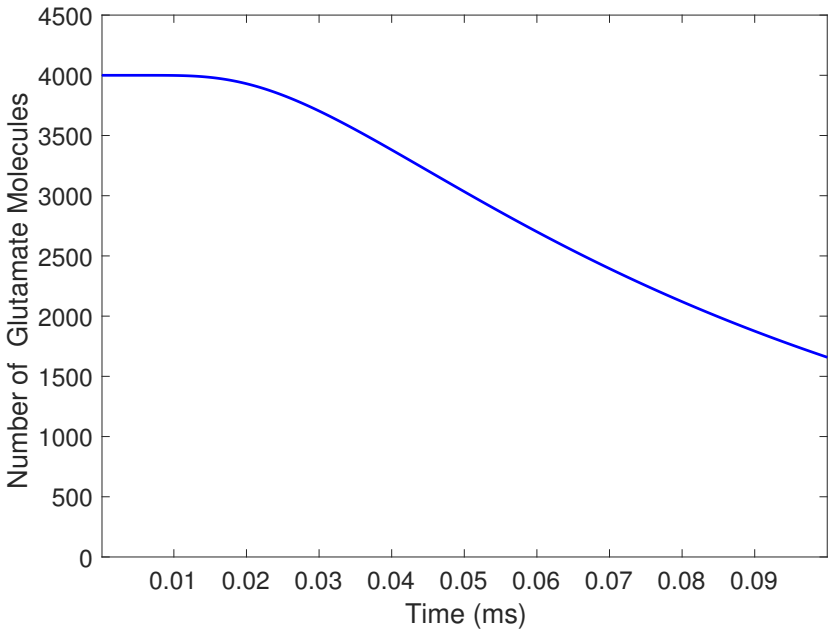

(a) Glutamates release near the center

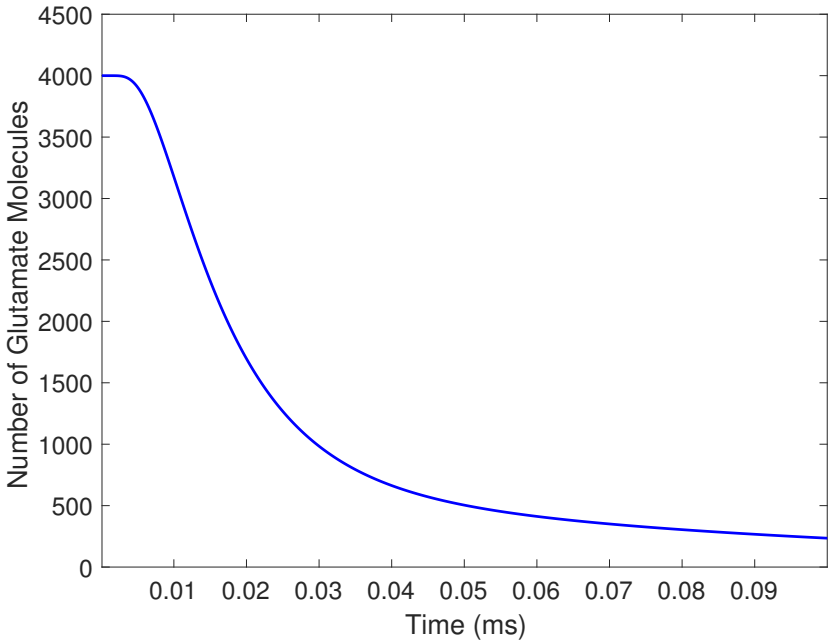

(b) Glutamates release near the edge

Figure 6.1: Total numbers of glutamate molecules within the cleft for 0.1 ms after an instantaneous release of 4000 glutamate molecules.

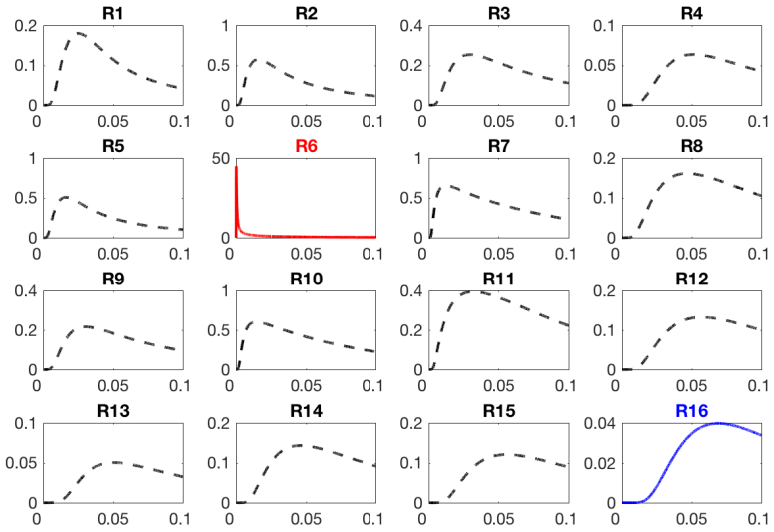

(a) Glutamates release near the center

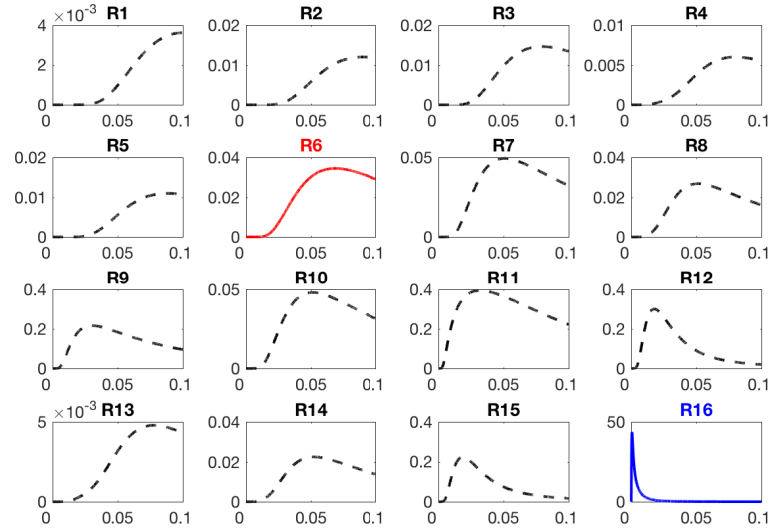

(b) Glutamates release near the edge

Figure 6.2: Glutamate concentration time series in $[0, 0.1]$ (unit: ms) for each location after 4000 glutamates are released.

Figure 6.2 shows concentrations of glutamate at each receptor location when 4000 glutamate molecules are released instantaneously at R6 near the center of the presynaptic terminal and released at R16 near the edge of the presynaptic terminal respectively (Figure 6.2a and 6.2b). Clearly, we can verify that the location over R6 has the highest glutamate concentration among 16 locations when center release occurs (Figure 6.2b). Analogously, the peak glutamate concentration appears at R16 receptor when an edge release occurs.

6.4 Piecewise Continuous Diffusion Coefficients

We consider an assumption that the background medium for glutamate diffusion might be different, depending on the location inside the cleft. We created an interior zone and an exterior zone where D_{glut} could vary zone to zone, it represents the inhomogeneity of material components in the cleft. Numerically, we verified that explicit finite difference scheme with piecewise continuous coefficients has accuracy of second order $O(h^2)$ for the synaptic diffusion problems.

6.4.1 Computation of Accuracy

The following data validates that the finite difference approximation is still applicable for our model with piecewise continuous coefficients across the boundaries of clefts and two zones.

We simulate three different models for releasing glutamate molecules. In the base model, we take $D = 0.4$ uniformly. In high affinity center model, we take $D^+ = 0.1$ in Ω^+ and $D^- = 0.4$ in Ω^-. Also in high affinity edge model, $D^+ = 0.4$ in Ω^+ and $D^- = 0.1$ in Ω^- are taken.

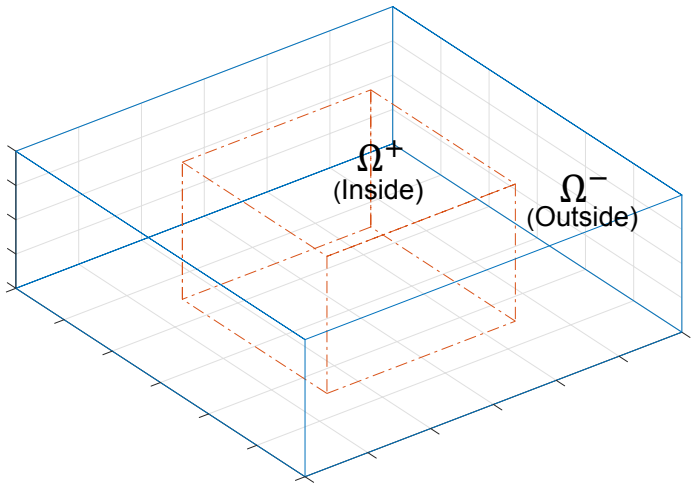

(a) Synaptic Cleft in 3-D

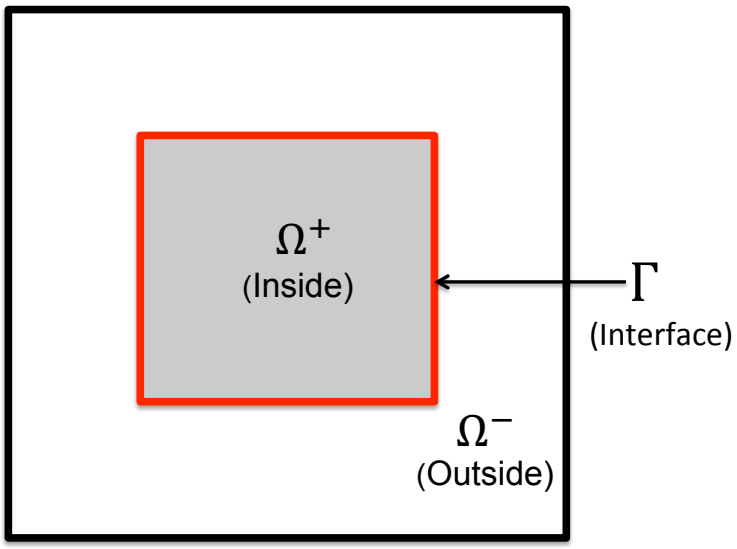

(b) Top View of Synaptic Cleft

Figure 6.3: The synaptic cleft space is divided into two zones. The diffusion coefficients takes two values in two regions(Ω^+ and Ω^-) respectively, which represent slow and fast motion of neurotransmitters in different material composition of the cleft space.

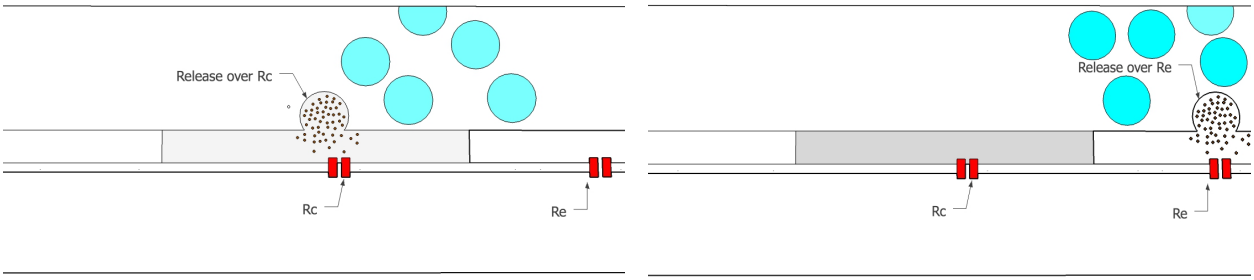

Figure 6.4: Front view of diffusion process with two different zones when center release(left) or edge release(right) occur at the cleft sites.

Since there is no exact solution with proper boundary conditions in our setting, we find the exponent of the error for our code by computation in our application problem.

We assume that $\Delta x = \Delta y = \Delta z$, and denote it $h = \Delta x$. We define

$$||E(n)||_\infty = \max_{i,j,k} |C_{i,j,k} - C'_{i,j,k}|, \tag{6.1}$$

where n is a number of nodes determined by $h(= \Delta x)$, and $C_{i,j,k}$, $C'_{i,j,k}$ are computed solutions with mesh size h and $\frac{h}{2}$ respectively.

Let $||E(n)||_\infty = O(h^p)$ and we estimate p based on errors in this problem. Let L is a the length of cubic domain, then

$$h = \frac{L}{n-1}.$$

We have

$$||E(n)||_\infty = (h^p) = O\left(\frac{L^p}{(n-1)^p}\right) \approx O\left(\frac{1}{n^p}\right).$$

We calculate $||E(n)||_\infty$ on different meshes(h, $\frac{h}{2}$, $\frac{h}{2^2}$). Then we denote n_1, n_2, and n_3 be the numbers of points on one side, and estimate the ratio

$$\frac{||E(n_2)||_\infty}{||E(n_1)||_\infty} = \frac{n_1^p}{n_2^p} \approx \left(\frac{n_1}{n_2}\right)^p, \tag{6.2}$$

and then solve for the order p by

$$p = \frac{\log(||E(n_2)||_\infty / ||E(n_1)||_\infty)}{\log(n_1/n_2)}. \tag{6.3}$$

D^+	D^-	$h(=\Delta x)$	$\Delta t(=A\cdot h^2)$	$D^+\frac{\Delta t}{(\Delta x)^2}$	$D^-\frac{\Delta t}{(\Delta x)^2}$	$\|\|E(n)\|\|_\infty$	p
0.1	0.4	0.02	8.00E-05	0.02	0.08	·	·
0.1	0.4	0.01	2.00E-05	0.02	0.08	2.5885816	·
0.1	0.4	0.005	5.00E-06	0.02	0.08	0.4199153	2.624
0.4	0.1	0.02	8.00E-05	0.08	0.02	·	·
0.4	0.1	0.01	2.00E-05	0.08	0.02	2.4116828	·
0.4	0.1	0.005	5.00E-06	0.08	0.02	0.4521747	2.451
0.4	0.75	0.02	8.00E-05	0.08	0.15	·	·
0.4	0.75	0.01	2.00E-05	0.08	0.15	1.7342439	·
0.4	0.75	0.005	5.00E-06	0.08	0.15	0.3581524	2.276

Table 6.1: Errors of solution and the order of accuracy p at diffusion mesh, time step, and diffusion coefficient

Where $\Delta t = A \cdot h^2$, A is a constant, in our case, we take $A = 0.2$. The CFL stability condition is $D\frac{\Delta x}{(\Delta x^2} < \frac{1}{8}$ in three dimensions[31]. Table 6.1 shows that when h is divided by 2, the error orders approximate to 2.4-2.6. This indicates that our numerical method is of second order accuracy.

6.5 Comparison of Two Models

We compare our model(Continuous Velocity Model) with the existing Support-Operator model (Harmonic Averaging). The relative discrepency for the total concentration is 0.2%, which indicates that there is no significantly difference between two models for total concentration. However, two models are taken different modelings on the interfaces, thus we

expect that concentrations depending upon locations might be different. We track glutamate concentrations at the specific locations beyond 16 NMDA receptors (R1-R16) and estimate the relative errors between two models as shown in Figure 6.6.

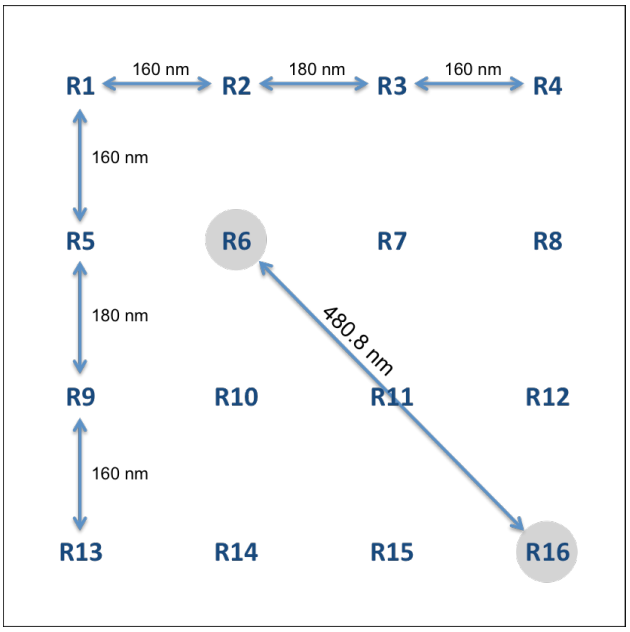

Figure 6.5: 16 NMDA receptors are evenly distributed on the postsynaptic terminal surface.

We simulate the glutamate release around R6 (Figure 6.5), then the glutamate molecules diffuse out and cross the interface to flush out of the cleft. R4, R13, and R16 produce the errors large than others. Nevertheless, the maximum relative error of 16 location is 2.9×10^{-2}, which is not significant for our problem as we are interested in relative ratio of opening probability. Figure 6.6 presents the comparative discrepancy of two models.

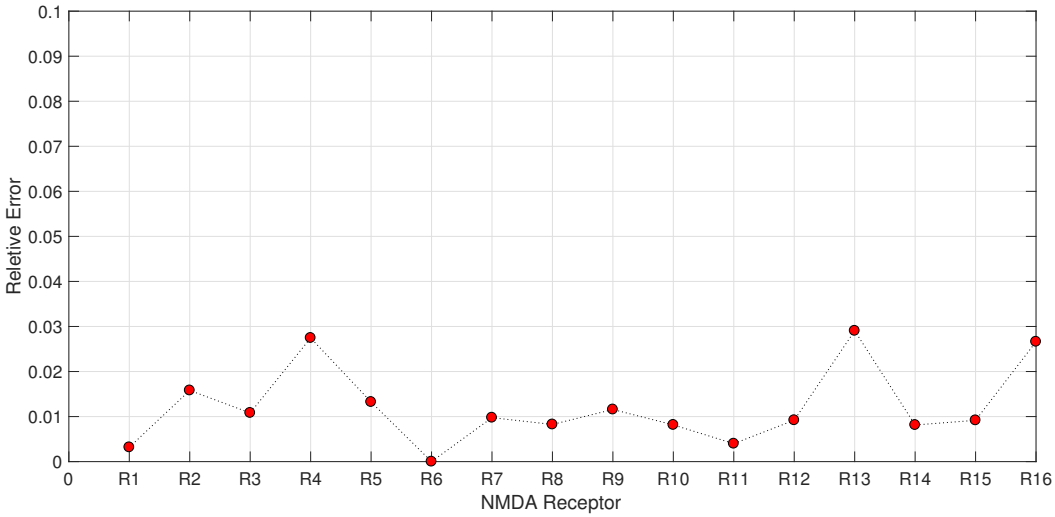

Figure 6.6: Relative discrepancy between Support-Operator and Continuous Velocity models of glutamate concentration over 16 NMDA receptors.

CHAPTER 7

Numerical Methods for Solving A System of Ordinary Differential Equations(ODEs)

7.1 Introduction

In this chapter, we study numerical methods for solving the Ordinary Differential Equation systems(ODEs). The differential equations are generally used to model time varying phenomena in science and engineering. To approach these complicated problems, we use numerical methods for approximating the solution of the original problem[7]. We first look at preliminaries of numerical methods and then study the Runge-Kutta method that we use to simulate our synaptic receptor model.

7.2 Runge-Kutta Methods

Definition 2. *If there exists a constant $L > 0$ such that*

$$|f(t, y_1) - f(t, y_2)| \leq L|y_1 - y_2|,$$

the function $f(t, y)$ is said to satisfy **Libschitz Condition** *when (t, y_1) and (t, y_2) are in $D \subset \mathbb{R}^2$. The constant L is called a* **Libschitz Constant** *for f.*

Definition 3. *A set $D \subset \mathbb{R}^2$ is* **convex** *if $(t, y_1), (t, y_2) \in D$, then*

$$((1 - \lambda)t_1 + \lambda t_2, (1 - \lambda)y_1 + \lambda y_2) \in D \text{ for every } \lambda \in [0, 1]$$

Theorem 1. *Suppose $f(t, y)$ is defined on a convex set $D \subset \mathbb{R}^2$. If a constant $L > 0$ exists with*

$$\left|\frac{\partial f}{\partial y}(t, y)\right| \leq L, \text{ for all } (t, y) \in D,$$

then f satisfies a Lipschitz condition on D in the variable y with a Lipschitz constant L.

The following theorem is the fundamental existence and uniqueness for the first order ordinary differential equations.

Theorem 2. *Suppose that $D = \{(t, y)|a < t < b, \ -Y < y < Y\}$, $Y > 0$ is fixed and that $f(t, y)$ is continuous on D. If f satisfies Lipschitz condition in D, then the initial value problem*

$$y'(t) = f(t, y), \ a \leq t \leq b, \ y(a) = y_0, \ |a_0| < Y.$$

has a unique solution $y(t)$ for $a \leq t \leq b$.

7.2.1 Euler's Method

This method is the most elementary numerical approach for solving initial value problems:

$$\frac{dy}{dt} = \phi(t, y), \ a \leq t \leq b, \ y(a) = y_0 \ , -Y < y_0 < Y. \tag{7.1}$$

Approximations to $y(t)$ are generated at finitely many points called **mesh points** in the interval $[a, b]$. When the approximation values are obtained at each point, the approximate solution at other points in the interval can be determined by interpolation.

Assume that the mesh points are equally distributed through the interval $[a, b]$ as following.

$$t_i = a + ih, \text{ for each } i = 0, 1, 2, \cdots, N - 1.$$

Here the distance between each pair of adjacent points $h = \dfrac{(b-a)}{N} = t_{i+1} - t_i$ is called the **step size**.

Using Taylor's Theorem, we derive Euler's method. Let $y(t)$ be the unique solution to 7.1, has continuous second-order derivatives on $[a, b]$, so that for each $i = 0, 1, 2, \cdots, N-1$,

$$y(t_{i+1}) = y(t_i) + hy'(t_i) + \frac{h^2}{2}y''(\xi_i), \text{ for } \xi \in (t_i, t_{i+1}).$$

From the Equation 7.1, we obtain

$$y(t_{i+1}) = y(t_i) + h\phi(t_i, y(t_i)) + \frac{h^2}{2}y''(\xi_i), \text{ for } \xi \in (t_i, t_{i+1}). \tag{7.2}$$

Let u_i is an approximation of the solution $y(t_i)$, we substitute u_i for $y(t_i)$ in Equation 7.2. The Euler's method is as follows,

$$\begin{aligned} u_0 &= a_0, \\ u_{i+1} &= u_i + h\phi(t_i, u_i), \text{ for each } i = 0, 1, 2, \cdots, N-1. \end{aligned}$$

7.2.2 Local Truncation Error

Numerical methods determine the accuracy of approximations. For this case, we consider the **local truncation error**.

For the initial value problem 7.1, the Euler method has **local truncation error** as following.

$$\tau_{i+1}(h) = \frac{y_{i+1} - (y_i + h\phi(t_i, y_i))}{h} = \frac{y_{i+1} - y_i}{h} - \phi(t_i, y_i) \tag{7.3}$$

for each $i = 0, 1, 2, \cdots, N-1$.

This error is a local truncation error because it measures the accuracy of the method at a specific step. Euler's method has

$$\tau_{i+1}(h) = \frac{h}{2}y''(\xi_i), \text{ for some } \xi_i \in (t_i, t_{i+1}).$$

If there exist a constant M such that $|y''(t)| \leq M$ on $[a, b]$, then this implies

$$|\tau_{i+1}(h)| \leq \frac{h}{2}M,$$

so the local truncation error in Euler's method is $O(h)$.

7.2.3 Taylor Method of Order n

First, we express the solution $y(t_{i+1})$ to the initial value problem in Theorem 2 by its n-th Taylor polynomial centered at t_i,

$$\begin{aligned} y(t_{i+1}) &= y(t_i) + hy'(t_i) + \frac{h^2}{2!}y"(t_i) + \cdots + \frac{h^n}{n!}y^{(n)}(t_n) + \frac{h^{n+1}}{(n+1)!}y^{(n)}(\xi), \text{where } t_i \leq \xi_i \leq t_{i+1} \\ &= y(t_i) + hf(t_i, y(t_i)) + \frac{h^2}{2!}f'(t_i, y(t_i)) + \cdots + \frac{h^n}{n!}f^{(n-1)}(t_i, y(t_i)) + \frac{h^{n+1}}{(n+1)!}f^{(n)}(\xi_i, y(\xi_i)) \\ &= y(t_i) + h\left(f(t_i, y(t_i)) + \frac{h}{2!}f'(t_i, y(t_i)) + \cdots + \frac{h^{(n-1)}}{n!}f^{(n-1)}(t_i, y(t_i)) + \frac{h^n}{(n+1)!}f^{(n)}(\xi_i, y(\xi_i))\right). \end{aligned}$$

Define

$$T^{(n)}(t, y(t_i)) = f(t_i, y(t_i)) + \frac{h}{2!}f'(t_i, y(t_i)) + \cdots + \frac{h^{(n-1)}}{n!}f^{(n-1)}(t_i, y(t_i)), \tag{7.4}$$

$$R_n(t_i) = \frac{h^n}{(n+1)!}f^{(n)}(\xi_i, y(\xi_i)). \tag{7.5}$$

Let u_i be an approximation of the solution $y(t_i)$, we substitute u_i for $y(t_i)$. In general, for $n \geq 1$, and $n \in \mathbb{N}$, the Taylor method defines:

$$\begin{aligned} u_0 &= y_0, \\ u_{i+1} &= u_i + hT^{(n)}(t_i, u_i), \text{ for each } i = 0, 1, 2, \cdots, N-1 \end{aligned}$$

where

$$T^{(n)}(t_i, u_i) = f(t_i, u_i) + \frac{h}{2} f'(t_i, u_i) + \cdots + \frac{h^{n-1}}{n!} f^{(n-1)}(t_i, u_i).$$

Therefore, Euler's method is Taylor's method of order one, i.e. $n = 1$.

7.2.4 Taylor Theorem in 2-dimensions

The Runge-Kutta method is a high-order method based on Taylor's method, but it does not require computing the derivative of $f(t, y)$.

Theorem 3 (Taylor's Theorem in Two Variables)**.** *Suppose that $f(t, y)$ and all its partial derivatives up to $n + 1$ order are continuous on $D = \{(t, y) | a \leq t \leq b, c \leq y \leq d\}$, and let $(t_0, y_0) \in D$. For every $(t, y) \in D$, there exists (ξ, μ), $t_0 < \xi < t$, and μ is between y and y_0, such that*

$$f(t, y) = P_n(t, y) + R_n(t, y),$$

where

$$\begin{aligned} P_n(t, y) = f(t_0, y_0) &+ \left[(t - t_0) \frac{\partial f}{\partial t}(t_0, y_0) + (y - y_0) \frac{\partial f}{\partial y}(t_0, y_0) \right] \\ &+ \left[\frac{(t - t_0)^2}{2} \frac{\partial^2 f}{\partial t^2}(t_0, y_0) + (t - t_0)(y - y_0) \frac{\partial^2 f}{\partial t \partial y}(t_0, y_0) + \frac{(y - y_0)^2}{2} \frac{\partial^2 f}{\partial y^2}(t_0, y_0) \right] + \cdots \\ &+ \left[\frac{1}{n!} \sum_{k=0}^{n} \binom{n}{k} (t - t_0)^{n-k} (y - y_0)^k \frac{\partial^n f}{\partial t^{n-k} \partial y^k}(t_0, y_0) \right] \end{aligned}$$

and

$$R_n(t, y) = \frac{1}{(n+1)!} \sum_{k=0}^{n+1} \binom{n+1}{k} (t - t_0)^{n+1-k} (y - y_0)^k \frac{\partial^{n+1} f}{\partial t^{n+1-k} \partial y^k}(\xi, \mu).$$

$P_n(t, y)$ is called the nth Taylor polynomial of two variables for the function f at (t_0, y_0) and $R_n(t, y)$ is the remainder term.

7.2.5 Runge-Kutta Method of Order Two

First, we need to determine a_1,α_1, and β_1 with the property that $a_1 f(t+\alpha_1, y+\beta_1)$ approximates

$$T^{(2)}(t,y) = f(t,y) + \frac{h}{2}\frac{df}{dt}(t,y). \tag{7.6}$$

The error does not exceed $O(h^2)$ because

$$f'(t,y) = \frac{df}{dt}(t,y) = \frac{\partial f}{\partial t}(t,y) + \frac{\partial f}{\partial y}(t,y)\cdot y'(t) \text{ and } y'(t) = f(t,y).$$

Then, we can write Equation 7.6 as

$$T^{(2)}(t,y) = f(t,y) + \frac{h}{2}\frac{\partial f}{\partial t}(t,y) + \frac{h}{2}\frac{\partial f}{\partial y}(t,y)\cdot f(t,y). \tag{7.7}$$

Now, we expand $f(t+\alpha_1, y+\beta_1)$ in its Taylor polynomial of degree 1 about (t,y).

$$a_1 f(t+\alpha_1, y+\beta_1) = a_1 f(t,y) + a_1\alpha_1\frac{\partial f}{\partial t}(t,y) + \alpha_1\beta_1\frac{\partial f}{\partial y}(t,y) + a_1\cdot R_1(t+\alpha_1, y+\beta_1), \tag{7.8}$$

where

$$R_1(t+\alpha_1, y+\beta_1) = \frac{\alpha^2}{2}\frac{\partial^2 f}{\partial t^2}(\xi,\mu) + \alpha_1\beta_1\frac{\partial^2 f}{\partial t\partial y}(\xi,\mu) + \frac{\beta^2}{2}\frac{\partial^2 f}{\partial y^2}(\xi,\mu),$$

and ξ is between t and $t+\alpha$ and μ is between y and $y+\beta$.

We match the coefficients of f and its derivatives in Equations 7.6 and 7.8, then it gives

$$\begin{aligned} a_1 &= 1; \\ a_1\alpha_1 &= \frac{h}{2}; \\ a_1\beta_1 &= \frac{h}{2}f(t,y) \end{aligned}$$

We obtain the parameters

$$a_1 = 1,\ \alpha_1 = \frac{h}{2}\ , \text{and } \beta_1 = \frac{h}{2} f(t,y),$$

$$T^{(2)}(t,y) = f\left(t + \frac{h}{2}, y + \frac{h}{2} f(t,y\right) - R_1\left(t + \frac{h}{2}, y + \frac{h}{2} f(t,y)\right),$$

$$R_1\left(t + \frac{h}{2}, y + \frac{h}{2} f(t,y\right) = \frac{h^2}{8}\frac{\partial^2 f}{\partial t^2}(\xi,\mu) + \frac{h^2}{4} f(t,y)\frac{\partial^2 f}{\partial t \partial y}(\xi,\mu) + \frac{h^2}{8}(f(t,y))^2 \frac{\partial^2 f}{\partial y^2}(\xi,\mu).$$

Therefore, if the second order partial derivatives of f is bounded, then $R_1\left(t+\frac{h}{2}, y+\frac{h}{2} f(t,y\right)$ is $O(h^2)$.

7.2.6 Third-Order Runge-Kutta Methods

Similarly, we can approximate $T^{(3)}$ with error $O(h^3)$ by

$$f(t + \alpha_1, y + \delta_1 f(t + \alpha_2, y + \delta_2 f(t,y))).$$

Four parameters are involved and we can use a method called Heun's method with $O(h^3)$.

$$\begin{aligned} u_0 &= a_0, \\ u_{i+1} &= u_i + \frac{h}{4}(f(t_i,u_i) + 3f(t_i + \frac{2h}{3}, u_i + \frac{2h}{3} f(t_i + \frac{h}{3}, u_i + \frac{h}{3} f(t_i,u_i)))), \\ &\quad \text{for } i = 0,1,2,\cdots,N-1. \end{aligned}$$

7.2.7 A 3(2) Pair of Runge-Kutta Formuli

Low order explicit Runge-Kutta methods are popular for solving initial value problems for a system of ordinary difference equations(ODEs). The key for low order formula is the availability of "free" interpolants that preserve monotonicity and convexity. Bogacki and Shampine proposed low order pairs of explicit Runge Kutta formulas that are either efficient, reliable, or more stable[5]. In order to obtain the numerical solution of our system

of ordinary differential equations, we take MATLAB solver ode23s that is effective with crude errors tolerance and relatively fast than other solvers[54].

CHAPTER 8

Simulations for NMDA Receptors on Postsynaptic Neuron

8.1 Introduction

In this chapter, we simulate the synaptic transmitter/receptor kinetic process by solving for a system of ODEs numerically, to obtain opening probabilities at NMDA receptors located in the post-synaptic terminal. We collect the data of open probabilities at NMDA receptors near the center release site or the edge release site, when evoked or spontaneous release occurs. We also consider additional factors such as size of synapse, geometric constriction, diffusion coefficient(different diffusivity inside cleft), and fusion pore to determine if any factor affects independent signaling between two modes of neurotransmission on NMDA receptors.

8.2 MATLAB Implementation

The glutamate concentration $C(x, y, z, t)$ simulating in chapter 6 was averaged over $10\mu s$ intervals (10 time steps) to reduce computational cost. MATLAB solver ode23s is effective at crude errors and relatively fast then other solvers[54]. Later, we also achieve the maximal open probability at select locations of a diagonal direction and vertical (or horizontal) direction in Figure 9.1, then define a function as the ratio of the maximum open probability of distal receptor over the maximum open probability of the release site (R_C or R_E). In this process the Piecewise Hermite Cubic Interpolation (PHCI) is used to

approximate the probable values for the function defined at discrete points so that we can preserve monotone or convex curve of the function[21].

8.3 Opening Probability at NMDA Receptor

We first simulate the glutamate release around the center site (R6), and obtain the opening probabilities at center (R6) and edge (R16) on the postsynaptic terminal. In chapter 6, we evaluated glutamate concentrations numerically by the Support-Operator model and the Continuous Velocity model, thus we have opening probabilities of NMDA receptor using the concentrations from the models.

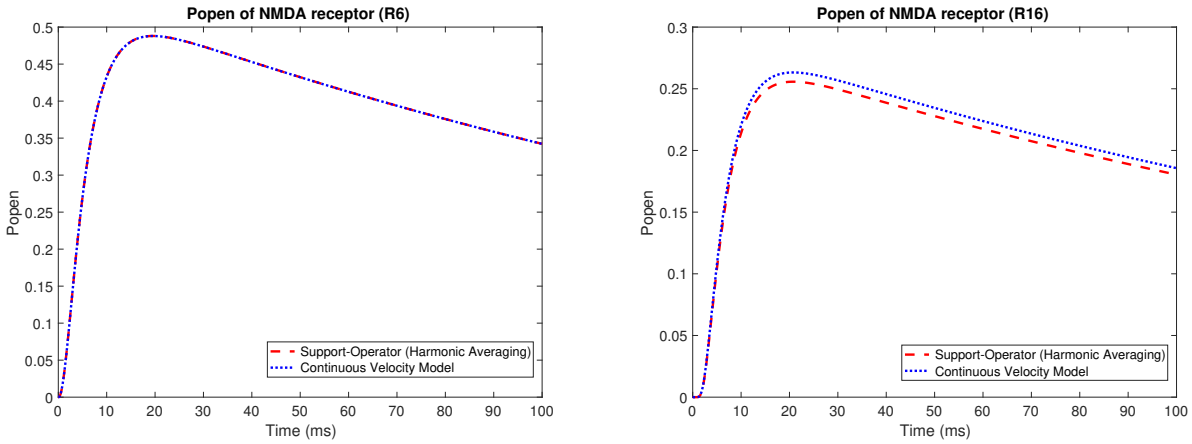

(a) P_{open} at R6 near center

(b) P_{open} at R16 near edge

Figure 8.1: NMDA receptor opening probability for center release

As shown in Figure 8.1, when glutamate molecules release near the center, then the maximum opening probability of NMDA receptor (R6) is 0.4880. The range of maximum opening probability of NMDA receptor (R16) near edge is 0.2557-0.2632. For errors of

opening probabilities between two methods do not make any significantly different outcomes, thus we will use only our new model (Continuous Velocity model) for following steps.

In Figure 8.1, this implies that glutamate release occurring at center site induces the higher opening probabilities at NMDA receptor(R6) directly opposing the center site than that of NMDA receptor(R16) near edge.

8.4 Effect of Synaptic Size

For large synapse(600nm by 600nm), the results in Figure 8.2 and 8.3 support recent experimental evidence that spontaneous and evoked currents are originated from released glutamate in different pools, accumulated at synapse center and edge respectively. As shown Table 8.1, we can verify that opening probability of NMDA receptor opposing the site of evoked release (center) is 0.4688 that is higher that that of spontaneous release(edge, 0.095) during evoked release at large synapse. This supports recent experimental result[49, 59] that two signals from spontaneous and evoked releases do not have crosstalk significantly.

As the size of synapse is smaller, the maximum open probability of the NMDA receptor opposing the corresponding site(either evoked release or spontaneous release) is decreasing. On the other hand, as the size of synapse is smaller, the maximum open probability of the NMDA receptor over the evoked site(spontaneous) around R6 is increasing when spontaneous release(evoked release) occurs because their distance in the same terminal postsynaptic is closer. This implies that the crosstalk of two modes of signals is increasing. This happens because in a small synapse, the glutamates are flushed out to external space quickly, so the opening probability would be lower at opposing locations. At this observation, for small synapse, we do not expect that spontaneous and evoked currents are originated from different pools in a single synapse since the degree of two modes of independency is very low.

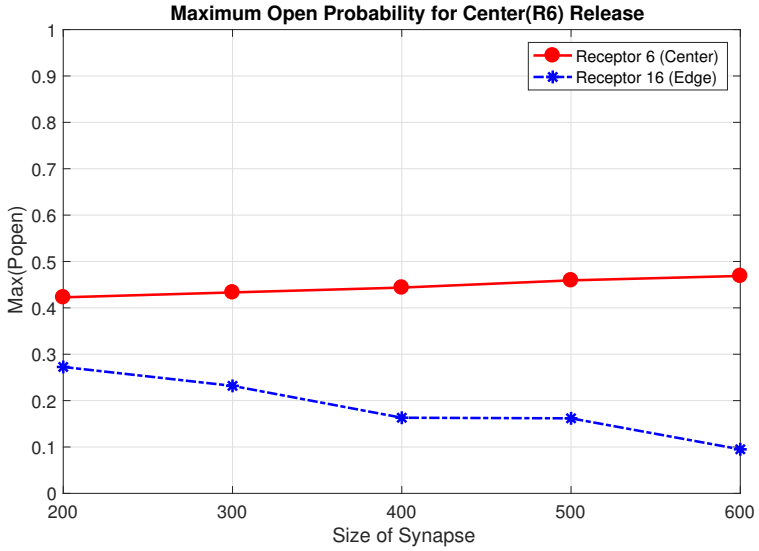

Figure 8.2: Center release: Max(P_{open}) of the NMDA receptor opposing the evoked release site (Red line) is higher than that of the NMDA receptor opposing spontaneous release site (Blue Line).

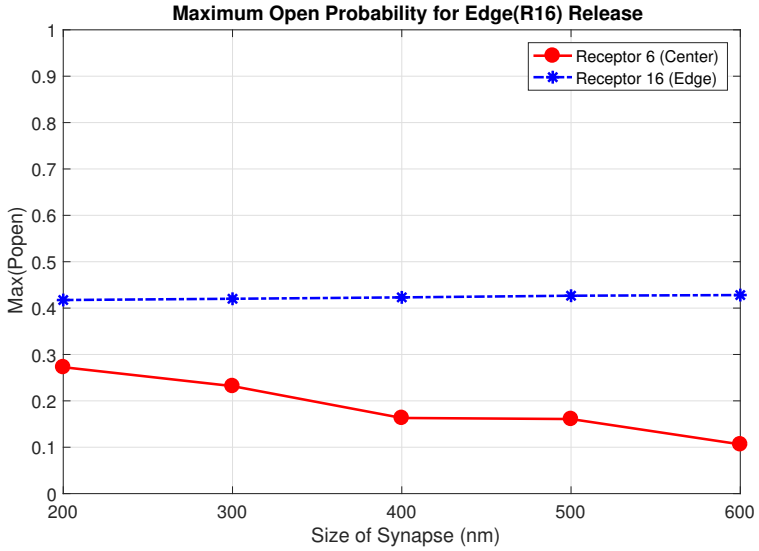

Figure 8.3: Edge release: Max(P_{open}) of the NMDA receptor opposing the spontaneous release site (Blue line) is higher than that of the NMDA receptor opposing evoked release site (Red Line).

Synaptic Size	Max(P_{open}) at Center	Max(P_{open}) near Edge	Ratio
200	0.4227	0.2726	1.5506
300	0.4333	0.2328	1.8612
400	0.4437	0.1631	2.7204
500	0.4593	0.1608	2.8563
600	0.4688	0.095	4.9347

Table 8.1: Center release: Maximal opening probability at center receptor and edge receptor when evoked release occurs at synapses of different size.

Synaptic Size	Max(P_{open}) at Center	Max(P_{open}) near Edge	Ratio
200	0.2726	0.4174	1.5311
300	0.2318	0.4201	1.8123
400	0.1631	0.4231	2.5941
500	0.1608	0.4267	2.6536
600	0.1062	0.4281	4.0310

Table 8.2: Edge release: Maximal opening probability at center receptor and edge receptor when spontaneous release occurs at synapses of different size.

8.5 Effect of Geometric Constriction

The space cleft between presynaptic terminal and postsynaptic terminal might not be void, nor uniform. The exact structure and composition of material vary from synapse to synapse. We test our model numerical simulating in two different geometries. In this case, we set the synaptic size as 600nm by 600nm. Illustrations in Figure 8.4 show how four situations are simulated. In narrow center geometry, the height is 10nm in center zone Ω^+, and height of the edge is 20nm in outside cleft Ω^-. The narrow edge geometry has 20nm in center and 10nm in edge(See Figure 6.3). Other conditions are same as the base model.

From the results presented in Figure 8.5, we find that there is no significant difference in conclusion. However, narrow center model produces slightly higher ratio for both evoked and spontaneous release. This is an indication favoring independency of two modes. Therefore,

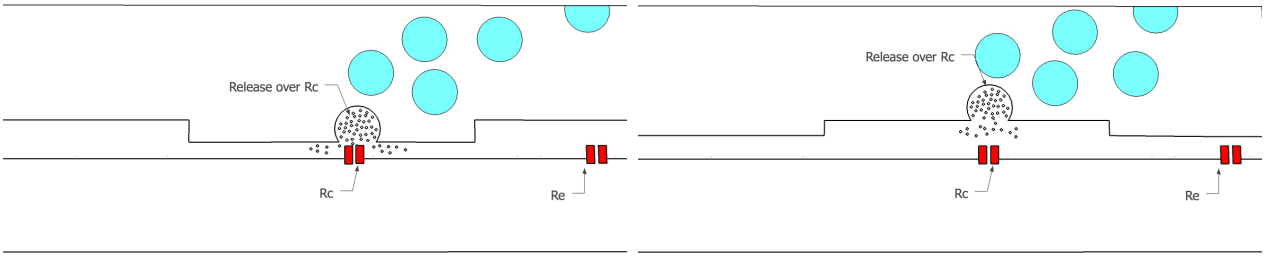

(a) Center release with narrow center

(b) Center release with narrow edge

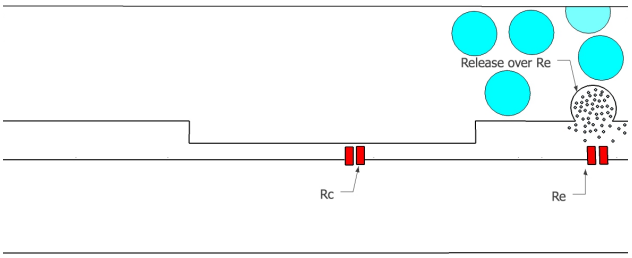

(c) Edge release with narrow center

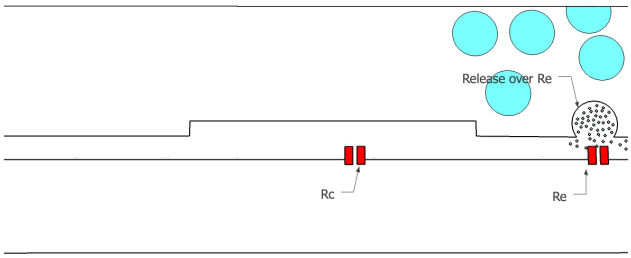

(d) Edge release with narrow edge

Figure 8.4: Illustration: Non-uniform space in the cleft

we conclude that the geometric constriction has no significant impact on the ratio of the maximum opening probability, and geometric constrict is not a significant factor.

Geometric Constriction	Max(P_{open}) at Center	Max(P_{open}) near Edge	Ratio
Flat(Base Model)	0.4688	0.1062	4.4143
Narrow Center	0.4657	0.0909	5.1232
Narrow Edge	0.4817	0.1082	4.4519

Table 8.3: Center release: Maximum opening probability at center receptor and edge receptor when the evoked release occurs for different synapse geometries.

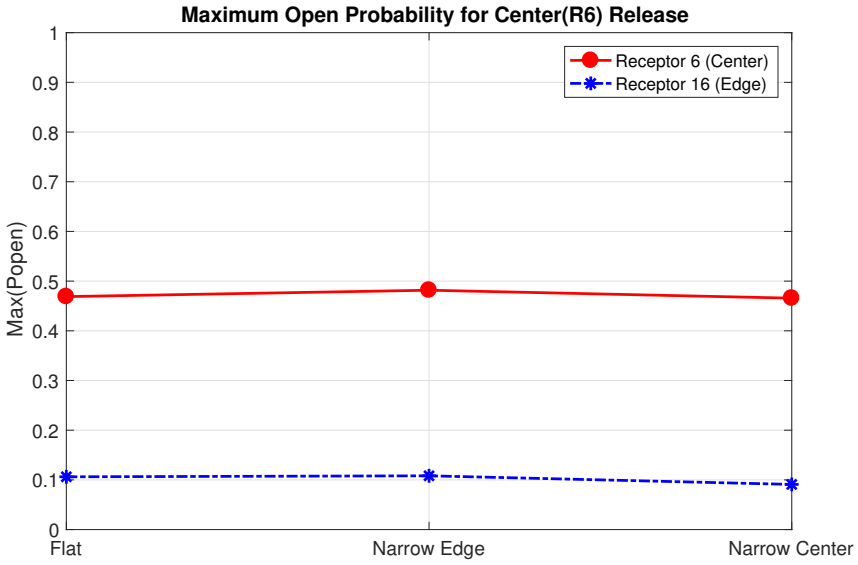

(a) Center release(R6)

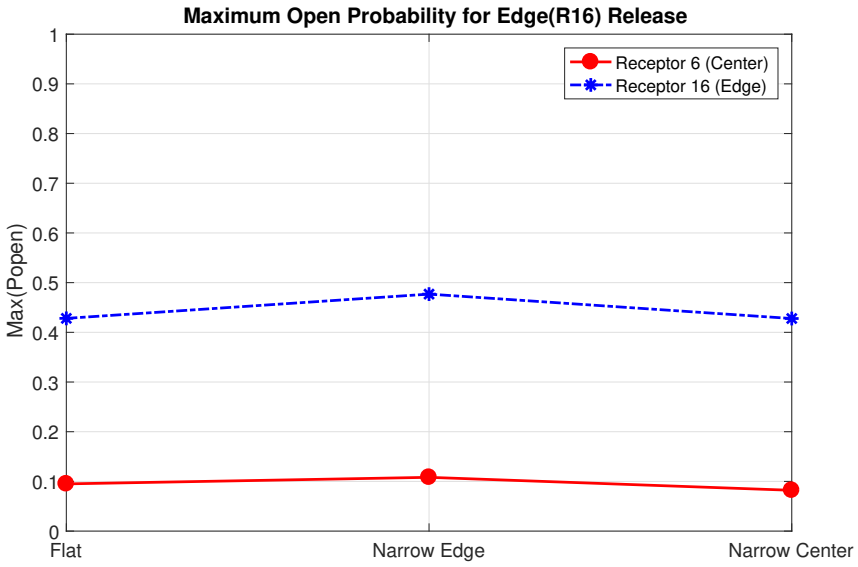

(b) Edge release(R16)

Figure 8.5: The maximal NMDA receptor opening probability Max(P_{open}) for geometric constriction in flat, narrow edge and narrow center cleft space.

Geometric Constriction	Max(P_{open}) at Center	Max(P_{open}) near Edge	Ratio
Flat(Base Model)	0.0950	0.4281	4.5063
Narrow Center	0.0821	0.4278	5.2107
Narrow Edge	0.1082	0.4769	4.4075

Table 8.4: Edge release: Maximum opening probability at center receptor and edge receptor when spontaneous release occurs for different synapse geometries.

8.6 Effect of Diffusion Inhomogeneity

The exact composition of materials in the cleft is not known. However, it is generally accepted the permeation of glutamate molecules can be described by a classical heat diffusion equation 4.1. We simulate three diffusion different models. In the base model, we take $D = 0.4$ uniformly. In high affinity center model, we take $D^+ = 0.1$ in Ω^+ and $D^- = 0.4$ in Ω^-. Also in high affinity edge model, $D^+ = 0.4$ in Ω^+ and $D^- = 0.1$ in Ω^- are taken as shown in Figure 6.4.

Diffusion Coefficients	Max(P_{open}) at Center	Max(P_{open}) near Edge	Ratio
Flat(Base Model)	0.4688	0.1062	4.4143
High Affinity Center	0.4845	0.0257	18.852
High Affinity Edge	0.488	0.2632	1.8541

Table 8.5: Center release: Maximum opening probability at center receptor and edge receptor when evoked release occurs for different zone diffusion models.

Diffusion Coefficients	Max(P_{open}) at Center	Max(P_{open}) near Edge	Ratio
Flat(Base Model)	0.0950	0.4281	4.5063
High Affinity Center	0.0244	0.4291	17.586
High Affinity Edge	0.2314	0.457	1.9749

Table 8.6: Edge release: Maximum opening probability at center receptor and edge receptor when spontaneous release occurs for different zone diffusion models.

When evoked and spontaneous releases occur, we find the ratio of two peak opening probabilities have 17-18 folds ratio, which is over three times than that of base model. We expect the situation that from entering zone to another zone, there might be a barrier, so that it is hard for glutamates to swim and move to another zone thus it favors independency of two modes of neurotransmission. This is compatible with the experimental results that the action potential evoked fusion is guided by the protein gradient called nanoclusters, which were more likely to active local NMDA receptors only, a fact noted in a recent paper published in Nature[59].

8.7 Effect of Narrow Fusion Pore

The instantaneous release of 4000 glutamate molecules is an approximation for the actual situation. The release of glutamate from vesicles in presynaptic terminals is a complex process that includes elevation of Ca^{2+}, binding of SNARE protein to the membrane and a sequence of events guided by biochemical reactions[56].

We model the limited rate release with additional components of a vesicle and a fusion pore inside the presynaptic terminal. The vesicle size is $40nm \times 40nm \times 40nm$. We test the glutamates release from 10nm diameter fusion pore (dimension $10nm \times 10nm \times 10nm$) for a regular fusion pore model, and the other narrower 2nm diameter fusion pore ($2nm \times 2nm \times 10nm$) as a slower release (See Figure 4.4). We then calculate receptor kinetics and find the maximal opening probability at each receptor. Figure 8.7 illustrates the results with a center release for evoked transmission and for spontaneous release at the edge. We compare the peak open probability ratio at center receptor and edge receptor respectively.

The results from the narrow fusion pore model, have a very big ratio of the peak opening probability of NMDA receptor directly opposing evoked site and spontaneous site.

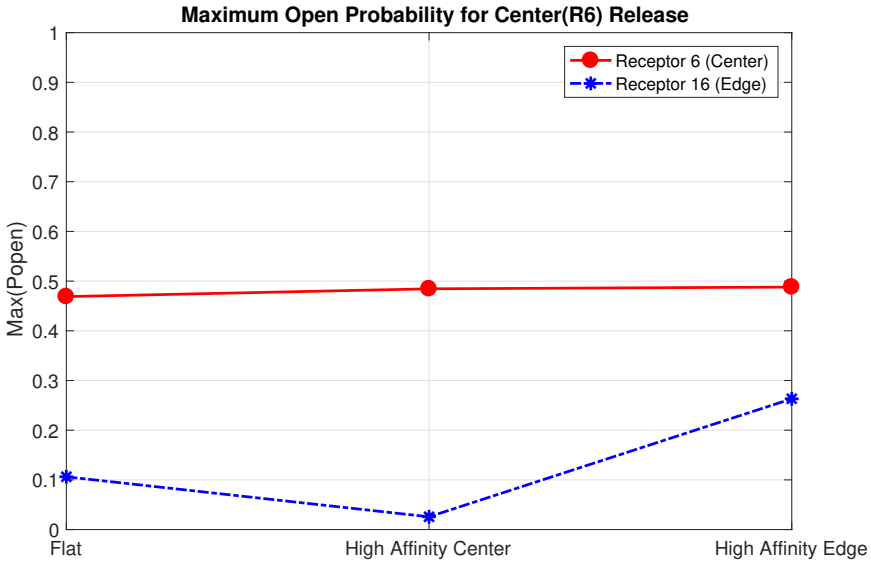

(a) Center release(R6)

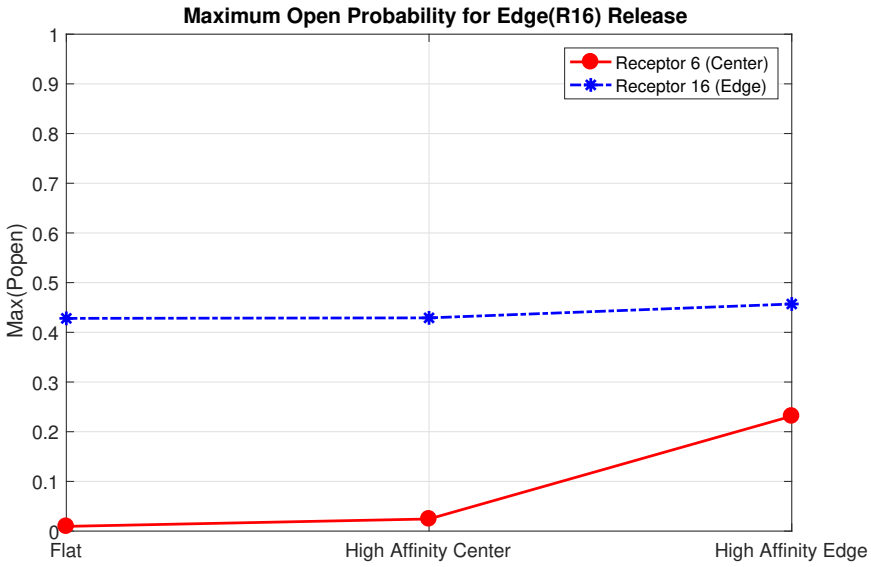

(b) Edge release(R16)

Figure 8.6: The maximal NMDA receptor opening probability Max(P_{open}) in various diffusion coefficients depending on locations in Ω^+, Ω^-.

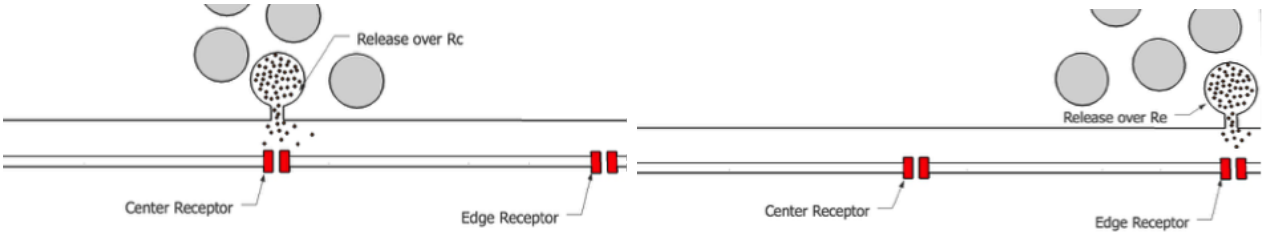

(a) Center release (b) Edge release

Figure 8.7: Diffusion process with 2nm or 10nm fusion pore.

For 10nm width of fusion pore, 77.6 folds difference of two modes, which agrees also the recent experimental evidence that two signals from spontaneous and evoked release are not correlated significantly. For 2nm fusion pore model drives 2238.9 folds as shown Table 8.7 for evoked release similar ratios observed for spontaneous release. We conclude that narrow fusion pore virtually assures the independency of two signals from spontaneous and evoked release.

Fusion Pores	Max(P_{open}) at Center	Max(P_{open}) near Edge	Ratio
Instantaneous(Base Model)	0.4688	0.1062	4.4143
10nm Fusion Pore	0.4422	0.0057	77.578
2nm Fusion Pore	0.1471	6.57E-05	2238.9

Table 8.7: Center release: Maximum opening probability at center receptor and edge receptor when evoked release occurs for different fusion pore.

Fusion Pores	Max(P_{open}) at Center	Max(P_{open}) near Edge	Ratio
Instantaneous(Base Model)	0.0950	0.4281	4.5063
10nm Fusion Pore	0.0057	0.4154	72.877
2nm Fusion Pore	6.57E-05	0.0833	1267.88

Table 8.8: Edge release: Maximum opening probability at center receptor and edge receptor when evoked release occurs for different fusion pore.

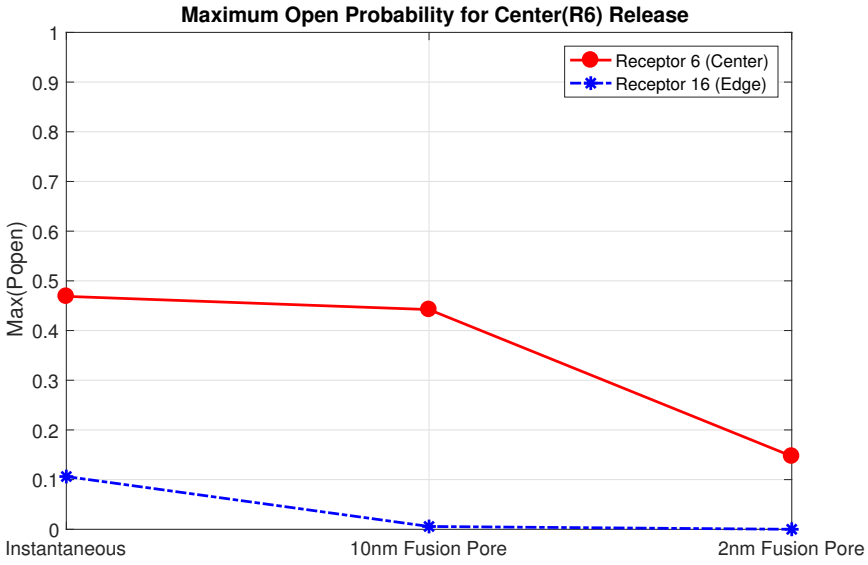

(a) Center release(R6)

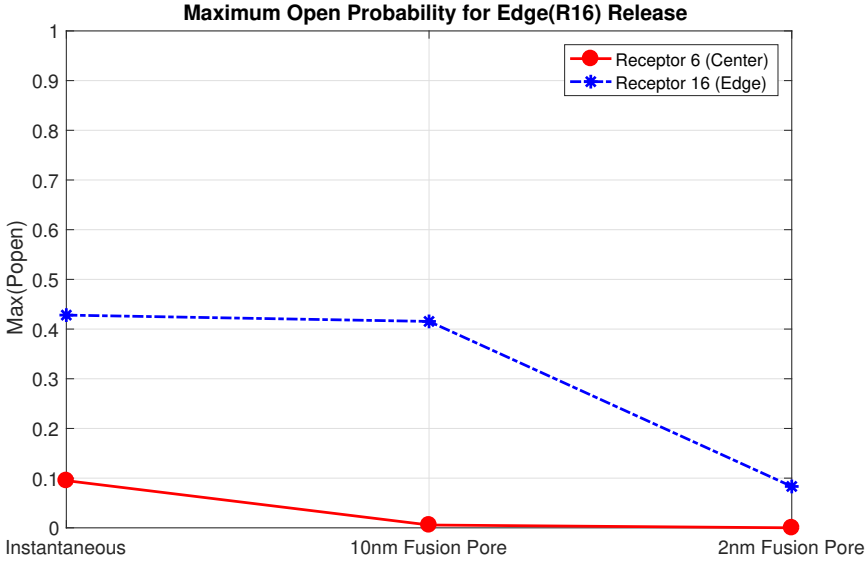

(b) Edge release(R16)

Figure 8.8: The maximal NMDA receptor opening probability Max(P_{open}) in different fusion pores, under (a) center release of glutamate molecules, (b) edge release of glutamate molecules.

CHAPTER 9

Results

In chapter 7, we simulated neurotransmission models considering factors as a synaptic size, geometric constriction, diffusion inhomogeneity, and a narrow fusion pore. We concluded that as a synapse size is smaller and if the cleft space is more cohesive in the peripheral area than the centre area, then there is a high possibility of having crosstalk of signals of spontaneous and evoked releases. On the other hand, when a synapse size is larger, the cleft space has more affinity in the central area than the edge area, and if the geometry of fusion has a narrower space, then it produces a better chance for independence of two currents.

The maximum open probability is most sensitive to the distance from the release sites. Using this property, we create a measurement of independency with combining factors that help to induce two independent signals from spontaneous and evoked transmissions in a single synapse. We can also estimate the distance between presynaptic release site and postsynaptic NMDA receptor based on presynaptic vesicle distribution and postsynaptic receptor density.

9.1 Measurement of Independency

We denote the relative ratio function as the ratio of the maximum open probability of distal receptor over the maximum opening probability of the receptor directly opposing the release site (center or edge). Respectively, we call a receptor as R_C, which is directly opposing

the evoked release site, and also represents a receptor located the center of postsynaptic terminal. A receptor R_E, directly opposing the spontaneous release site, is located around the edge of the postsynaptic terminal. The measurement 9.1 is showing the points where ratio functions are taken for comparison:

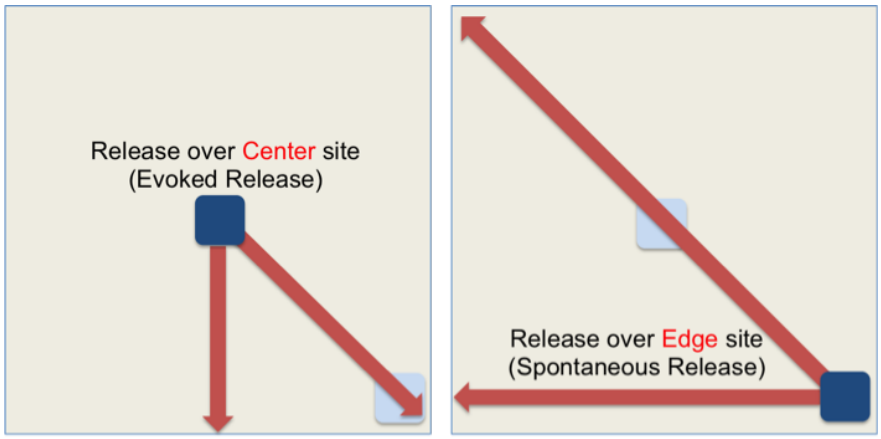

Figure 9.1: Two directions P_{open} at each location when center release (left) or edge release (right) occur their sites, and the NMDA maximal opening probability is calculated to test independency.

$$Measure := \frac{\text{Max}(P_{open}) \text{ at distal receptor}}{\text{Max}(P_{open}) \text{ at release site } (R_C \text{ or } R_E)}. \tag{9.1}$$

When we simulate our model, we fix the denominator as one receptor either R_C and R_E. Then we measure $\text{Max}(P_{open})$ at a receptor along the two directions as shown in Figure 9.1. The $\text{Max}(P_{open})$ in other locations will be valued between the values obtained in these two directions. If the steepness of function for ratio is relatively large, it implies that the evoked and spontaneous currents have a less chance of having crosstalk.

We use our measurement (9.1) to estimate the independency with considering effective conditions for independency such as a synaptic size, diffusion inhomogeneity, and fusion

pore. When glutamate vesicle releases over the center receptor in Figure 9.1 (left), for the receptors of equal distance to release, the diagonal direction shows the largest P_{open} and vertical (or horizontal) direction shows the smallest given the same distance.

9.2 Simulation Results

We use the model to calculate and compare three sizes of synapses as large synapse, medium synapse, and small synapse. Then we set areas of synapse as 600nm x 600nm for large synapse, $400nm \times 400nm$ for medium size, and $200nm \times 200nm$ for small synapse respectively. We estimate the minimum distance between two sets of NMDA receptors to have possible less crosstalk. The ratios of maximum opening probabilities are plotted in Figure 9.2a and 9.2b.

Based on the criteria from previous research [3, 49], we assume 5-fold is the threshold ratio as a good indicator for independent currents. We cannot assure independency with the structure evoked at center and spontaneous at edge for medium ($0.16\mu m^2$) and small synapses ($0.04\mu m^2$) in our current base model. For medium synapse ($400nm \times 400nm$), if two forms of release locate towards opposite corners of the synaptic cleft, we might achieve sufficient low level of crosstalk and possibly obtain the independence of spontaneous and evoked neurotransmissions [3]. For small synapse ($200nm \times 200nm$), there are apparently have more crosstalk between evoked and spontaneous releases.

We consider other constraints to find favorable conditions where the signals can be independent. One way is to assume the components in the cleft to be different compositions. We make the center area to be less diffusive for glutamate molecules than the peripheral region inside cleft. Another possibility is to reduce the amount of glutamate molecules

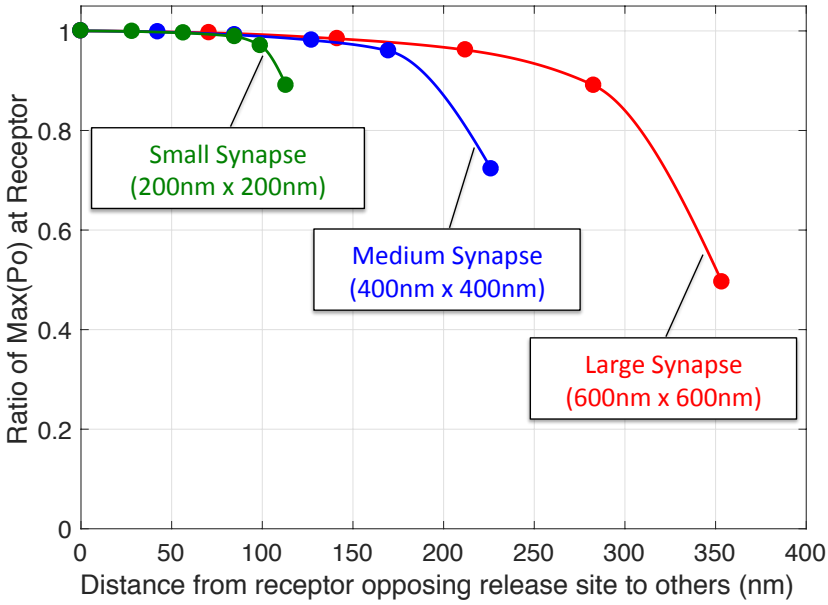

(a) Center release

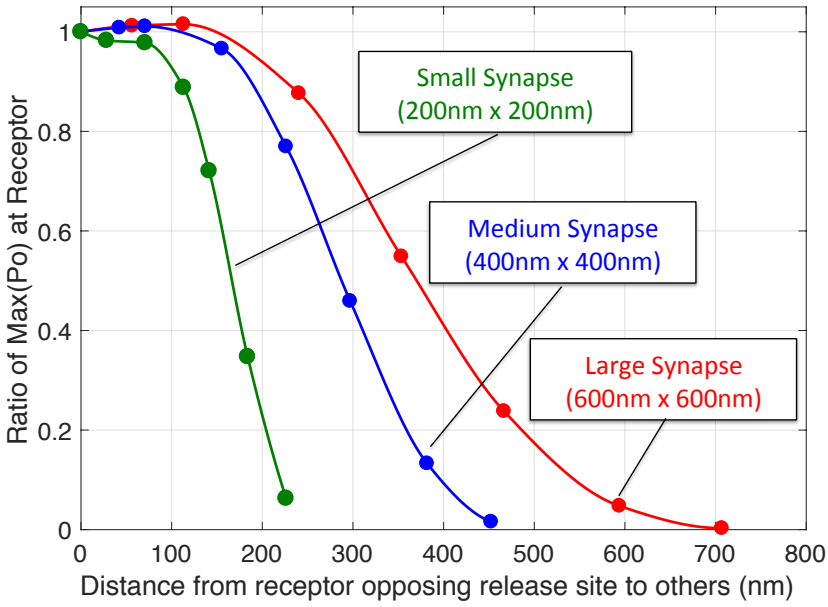

(b) Edge release

Figure 9.2: Ratio of Max(P_{open}) as a function of receptor distance for three synapse sizes.

released per vesicle in the partial release (called kiss-and-go) scenarios, and/or the glutamate is released in slower release rate due to partial opening of vesicles in the membrane.

9.2.1 Possible Scenario 1 : High Affinity Center in the Cleft

In Figure 9.3, among three lines for both evoked and spontaneous release, the high affinity center model has the sharper downward slope when the distance is apart. This is compatible with the recent experimental results that the evoked release is guided by the protein gradient and prefer to occur in confined area with in high local density of Rab3-interacting molecule(RIM)[59] in center area. However, from 0 to 150nm range of distance, all three lines are virtually constants as shown in Figure 9.3a, and this implies that this high affinity center is not enough for a small synapse to house the independent currents from two modes transmissions.

9.2.2 Possible Scenario 2 : Narrow Fusion Pores on the Presynaptic Sites

As shown in Figure 9.4, the limited vesicle fusion rate has impact on reducing the crosstalk of two currents from spontaneous and evoked releases. They did not impact as much to perturb the independent signaling of synapse on large synapses, although slower releases did promote more independence. They benefit small size synapses substantially more in achieving independent signaling. Figure 9.4e and 9.4f show that small synapse (200nm by 200nm) might not have independent signaling when evoked glutamate release occurs instantaneously because evoked and spontaneous release sites are not far away from each other and thus they have high probability of having crosstalk between each other. In fact, there is not much difference between the peak opening probabilities at a receptor for evoked release and the one for spontaneous release. This can be verified in the graph of Figure 9.4e,

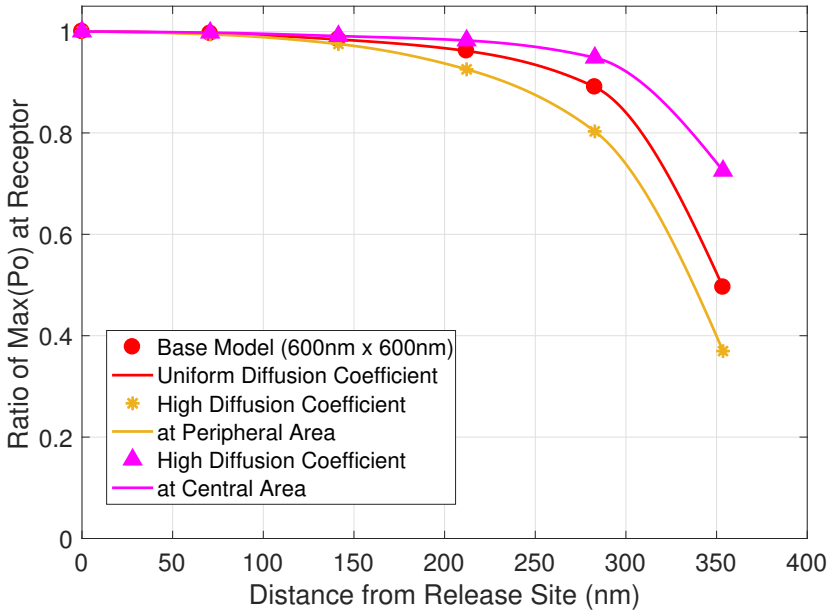

(a) Center release

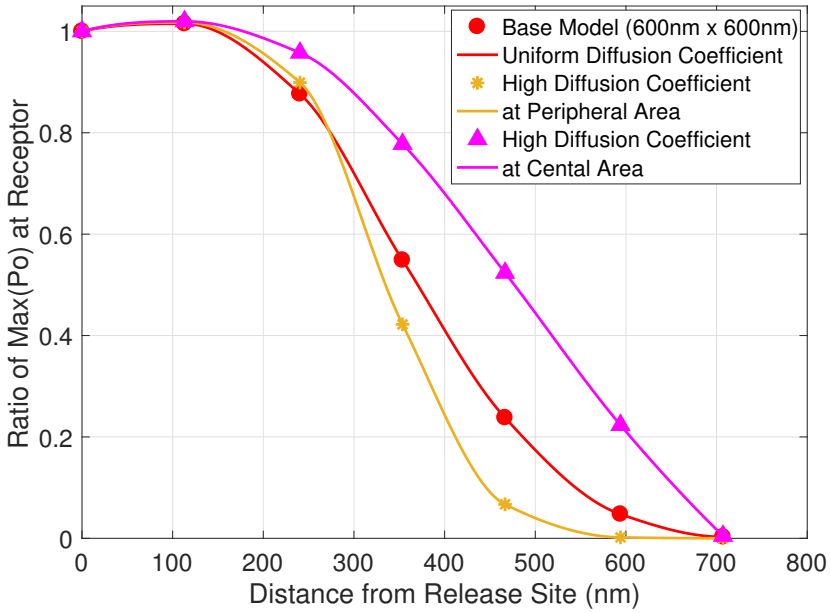

(b) Edge release

Figure 9.3: Ratio of Max(P_{open}) as a function of receptor distance for diffusion inhomogeneity(base, high affinity center, and high affinity edge)

the ratio of two maximum open probabilities is close to 1. The peak open probability in receptors is consistent up to 90nm far from the receptor molecules opposing evoked release site. However for small synapses, as glutamate release through 10nm and 2nm vesicle fusion pore, the open probability ratio decreases more drastically and becomes close to zero, and in 2 nm pore, the ratio achieves 10-fold reduction at 90nm distance, giving plausibility for independent currents from two transmissions.

9.3 Comparison with Biological Results

Most recent experiments in Dr. Kavalali's lab showed in mammalian synapses, spontaneous and evoked glutamate release driven NMDA receptor mediated Ca2+ transients often occur at the same synapse, but these two signals do not show significant correlation or crosstalk[49]. Also, Tang and colleagues proposed an alignment of presynaptic and postsynaptic nanoscale subdomains, called nanocolumn[59].

Evoked fusion occurs in confined areas by protein gradient with higher local density of Rab3-interacting molecules (RIM) within the presynaptic active zone. These RIM nanoclusters align with concentrated postsynaptic receptors. Evoked neurotransmitter release prefer to occur at sites directly opposing postsynaptic receptor guided by the nanoachitecture of the active zones. They estimated that majority(72-82%) of evoked signals arose from single vesicle fusion. The concentration of vesicle priming proteins in nanoclusters prefers to evoked fusion in the subregion of the active zone.

They showed three RIM 1/2 nanoclustes and three PSD-95(Post Synaptic Density) nanoclusters are well aligned for two pairs and not aligned for one pair. They used two independent approaches to estimate the relationship between active zone and postsynaptic density(PSD) protein distributions. In order to figure out of the trend, they measured

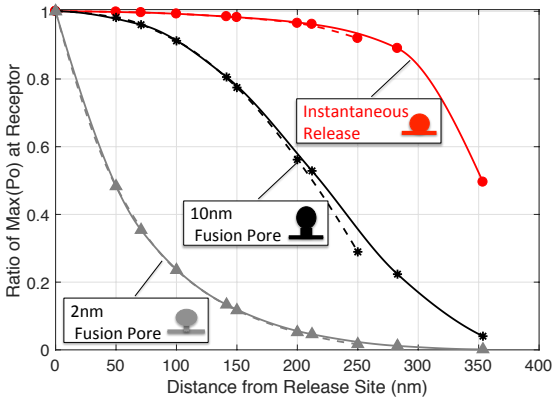

(a) Center Release for Large Synapse

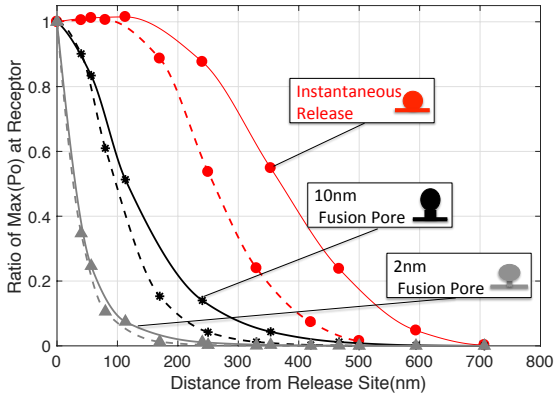

(b) Edge Release for Large Synapse

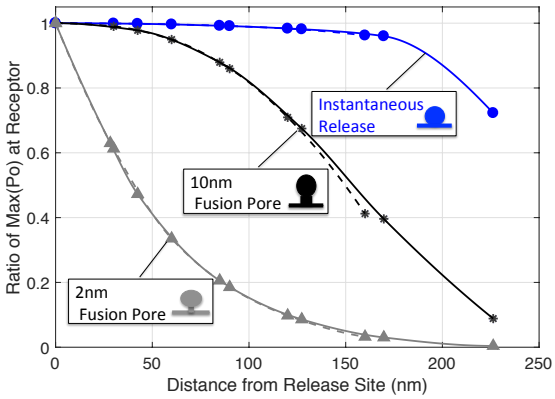

(c) Center Release for Medium Synapse

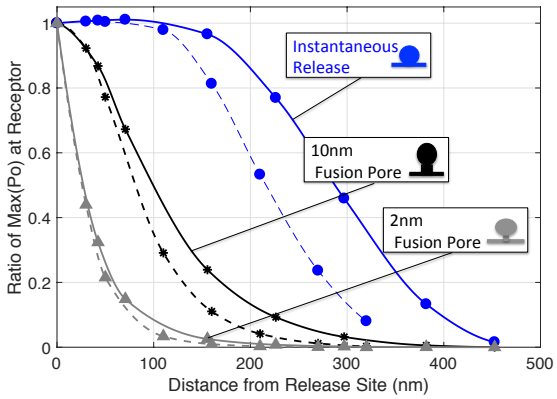

(d) Edge Release for Medium Synapse

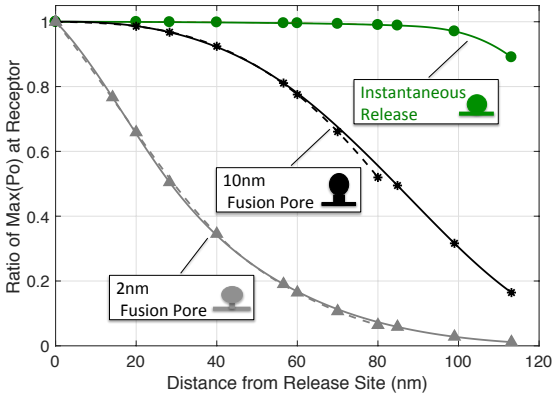

(e) Center Release for Small Synapse

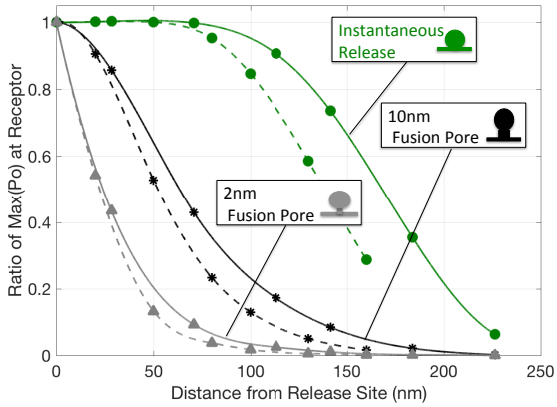

(f) Edge Release for Medium Synapse

Figure 9.4: Ratios of maximal NMDA receptor opening probabilities as functions of receptor distance for different release speed of glutamate vesicle release. The open probabilities were calculated by the kinetic equation for three types of size of synapse, when glutamate are released above the center and the edge respectively.

RIM 1/2 localization densities as a function of radial distance from the centres of PSD-95 nanoclusters as translated across the synaptic cleft. Similarly, they estimated PSD-95 protein enrichment densities as a function of the center of RIM 1/2 nanoclusters. Through this results, they defined an enrichment index as the average molecular density of the opposed protein (n=265-272) within a 60nm radius from the nanocluster center. They verified from this results if synapses are trans-synaptically aligned on the nanoscale level, the distribution of protein on side of the synapse may predict protein density in the opposing neuron.

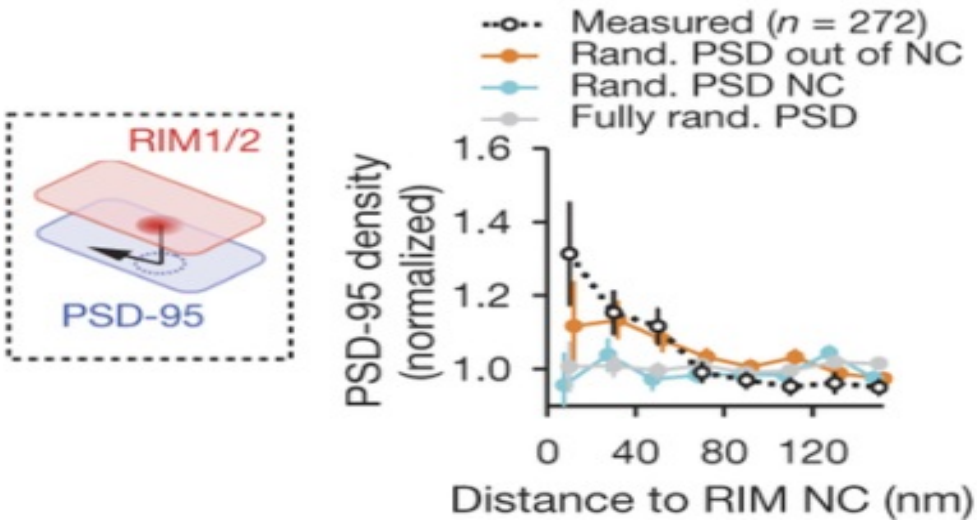

Figure 9.5: PSD-95 enrichment as a function of distance from translated RIM 1/2[59].

Their experimental findings are significantly relevant to our mathematical results. Thus, we compare their measured data with the result from our mathematical measurement for small synapse(200nm by 200nm).

We search out and approximate the data from Tan's team [**?**] and fitted with the exponential model using MATLAB. Figure 9.6a has trends of exponentially decreasing. Let

$$f_{PSD-95}(x) = a \cdot \exp(b \cdot x) \tag{9.2}$$

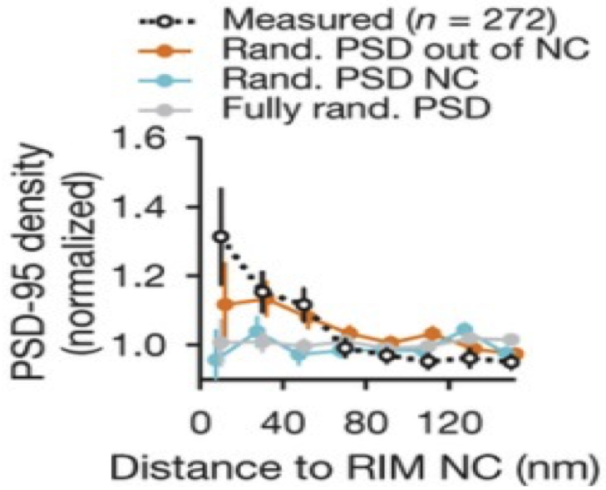

(a) Original Figure in [59]

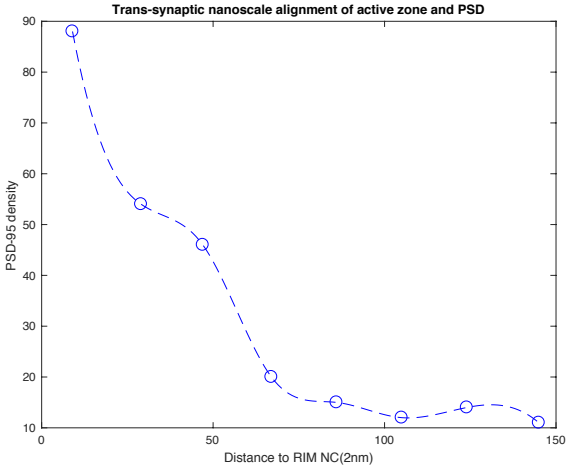

(b) Searched out measured data(n=272) from the left

Figure 9.6: PSD-95 enrichment as a function of distance from translated RIM 1/2[59] (left(a)) and searching out the measured data and plotting by MATLAB. Fitted the data with a general exponential model $f_{PSD-95}(x) = 104 \cdot \exp(-0.02038x)$(right (b)).

Then, we estimate the coefficients with 95 % confidence bounds of a is 104 (87.06, 121) and b is to -0.02038 (-0.02518, -0.01558). Therefore, this measured data of PSD-95 enrichment on the postsynaptic neuron as a function of distance relative to the center of RIM 1/2 nanocluster on presynaptic terminal is approximating to the exponential function as below:

$$f_{PSD-95}(x) = 104 \cdot \exp(-0.02038 \cdot x). \tag{9.3}$$

Now, let us remind possibility 2. We tested our simulation and suggested that we may obtain the independency of two currents from evoked and spontaneous neurotransmitter release when if small synapses have a geometry of a narrow fusion pore (2nm)(Figure 9.4f). The ratio achieves 10-fold reduction at 90nm distance, giving plausibility for independent currents from two modes of transmissions. This corresponds to the result of an enrichment

index within a 60nm radius from the nanocluster centre. Thus, we also consider the graph of ratio function of peak opening probability as a function of distance from the center synapse for small synapse and evoked narrow fusion pore release in Figure 9.7. Then we fit the graph to the exponential model similarly. The coefficients with 95 % confidence bounds of a is 1.044 (0.9322, 1.156) and b is approximating to -0.02791 (-0.03409, -0.02171). We obtain one exponential function for our simulation,

$$f_{simulation}(x) = 1.044 \cdot \exp(-0.02791 \cdot x). \tag{9.4}$$

The results are incredibly well-matched to each other, thus we rescale the coefficients of f_{PSD-95} and plot those two functions together(Figure 9.8). Also this indicates that small synapses might be conducted of dynamic functional modules and possibly hold the segregation of sites for spontaneous versus evoked neurotransmission within individual synapses. These results show our mathematical modeling is valuable and has capability to deal with the neuroscience challenging.

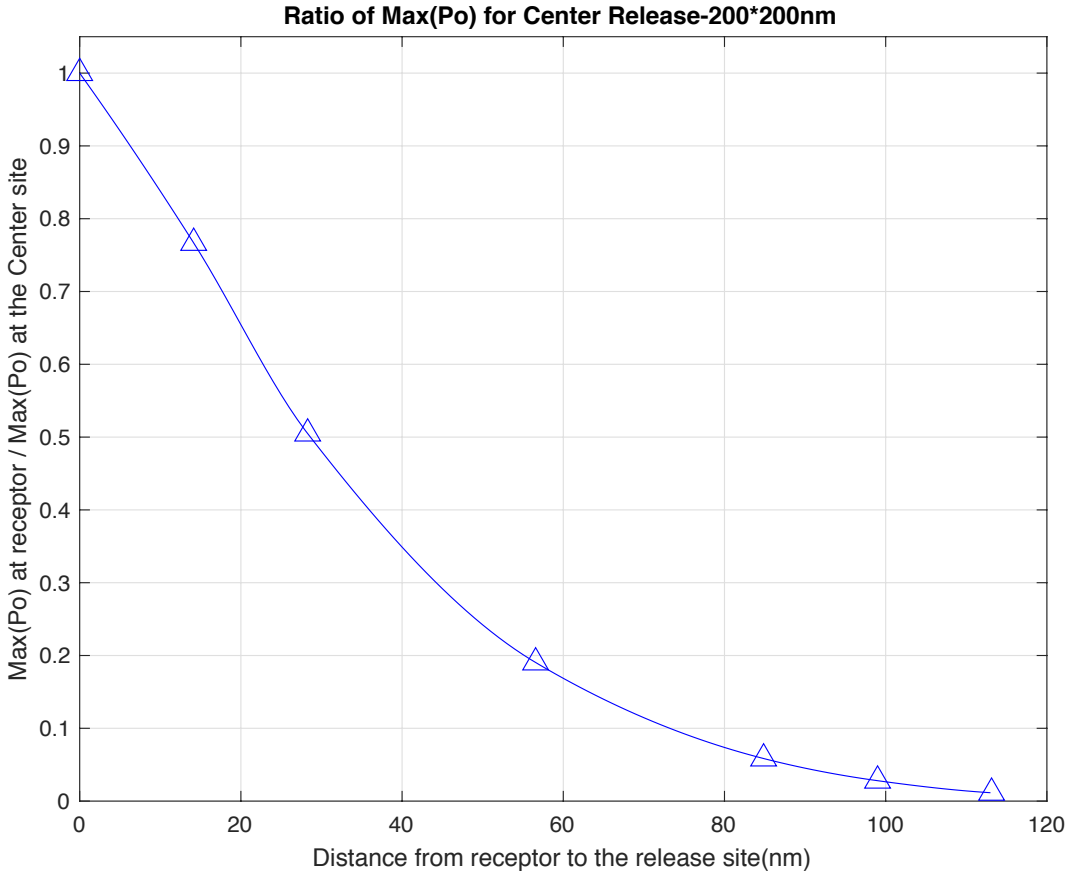

Figure 9.7: Our simulation: Ratio of Max(P_{open}) as a function of distance from the receptor opposing the evoked glutamate fusion pore (2nm) release site for small synapses (200nm by 200nm). Fitted the calculated data with a general exponential model $f_{simulation}(x) = 1.044 \cdot \exp(-0.02791x)$.

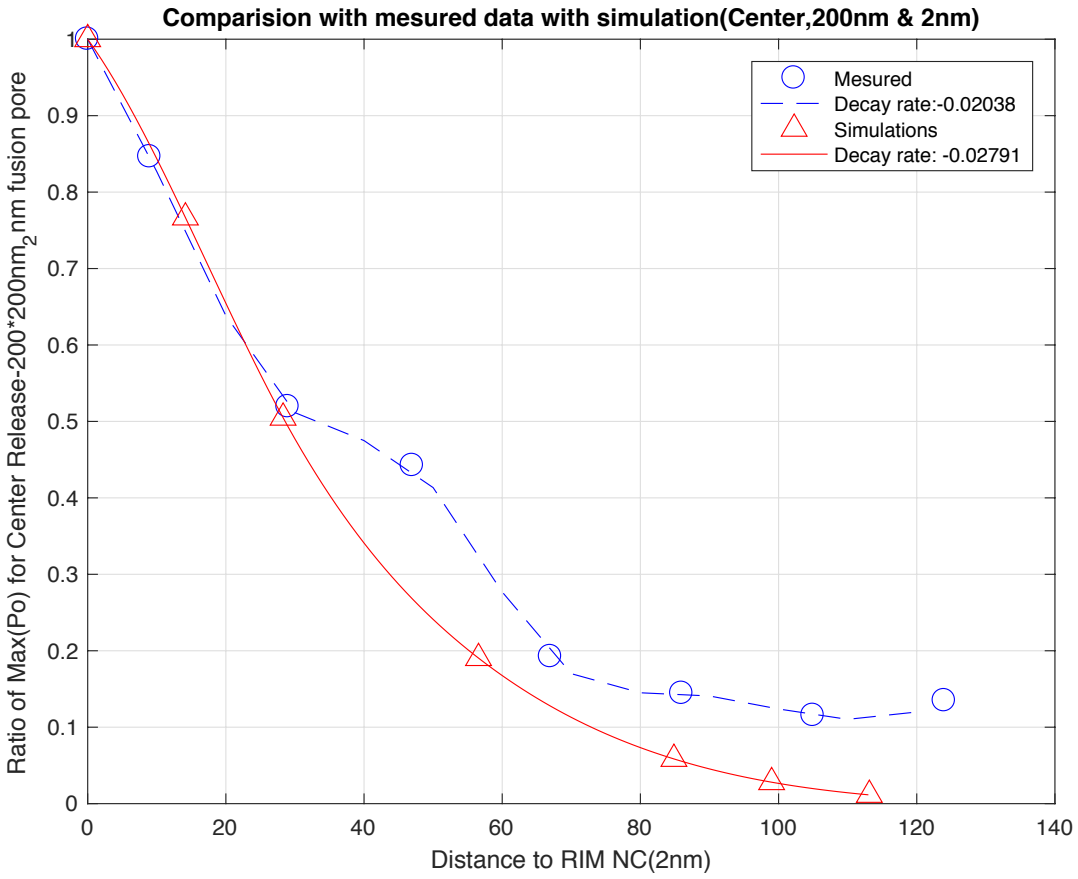

Figure 9.8: Rescaling measured data(PSD-95 Enrichment) and our simulation of ratio of Max(P_{open}) as a function of distance from the center of a synapse.

CHAPTER 10

Conclusions and Future Work

10.1 Summary

In chapter 2, we introduced basics of neuroscience and how synapses work in order to understand current questions that we need to consider. In chapter 3, we reviewed some preliminaries, such as low of mass action, enzyme kinetics process, and heat(diffusion) equation and its fundamental solution. In chapter 4, we developed a mathematical modeling of this synaptic-dynamics, and discussed some factors as our parameters that we will consider to solve the questions, such as boundary conditions, geometry of synapse, synaptic size, different glutamate diffusive rate in the cleft, and release rate of neurotransmitters from presynaptic terminal. In chapters 5 and 6, we studied finite difference methods to approximate solutions to heat equations in the process from presynaptic sites to the cleft. We also developed two numerical methods for solving the piecewise continuous heat diffusion equation in three dimensional space for a cubic domain, and proved its second order accuracy theoretically. Then we derived the MATLAB implementation of our presynaptic release model and simulated the process of glutamate release from presynaptic sites into the synaptic cleft to obtain glutamate molecules concentration at each receptor. We also applied our numerical method with piecewise continuous diffusion coefficients to the diffusion process and validated the method for second order truncation error. In chapters 7 and 8, we studied numerical methods of system of ordinary differential equations, especially Runge-Kutta methods, that we use to solve our system of 7 odes numerically. Then we simulated the kinetic process by

solving a system of ODEs numerically to obtain the opening probability at NMDA receptor. We considered factors as synaptic size, geometric constriction, diffusion inhomogeneity, and fusion pore size. We concluded that as a synaptic size is smaller and if the cleft space is less diffusive in the edge area than the centre area, then there is a higher possibility of having crosstalk of two signals from spontaneous and evoked release. On the other hand, when a synaptic size is larger, the cleft space is less diffusive in the central area than the edge area, or if the geometry of fusion has a narrower center, then those produce a better chances of independence of two modes of currents from spontaneous and evoked release. In chapter 9, we defined a measurement of independency and suggested two possible scenarios for small synapses to be less crosstalk from spontaneous and evoked neurotransmitter currents on postsynaptic terminals. In addition, we compared the recent experimental findings with our mathematical results for small synapse (200nm by 200nm). The results were incredibly well-matched to each other and this indicates that small synapses might be conducted of dynamic functional modules and possibly hold the segregation of sites for spontaneous versus evoked neurotransmission within an individual synapse. These results suggest that our mathematical modeling is valuable to solve neuroscience challenging.

10.2 Conclusion

In this dissertation, we developed a three dimensional mathematical model of a synapse to identify the spatial relationship between spontaneous and evoked neurotransmitter release for their segregation of currents. This research continues collaborative work of my advisor Dr. Su and Dr. Kavalali's group[3]. The major contribution of this research is following.

1. We developed a three dimensional mathematical model, so that we are able to analyze those results for independent signaling of spontaneous and evoked glutamate releases in

a synapse, comparing with the experimental and theoretical prediction of Dr. Kavalali lab. We defined a measurement of independency and set a criterion of subjectively a 5 fold ratio as a reasonable boundary for the independence. From those results we suggested two possibilities for small synapses to be less crosstalk from spontaneous and evoked neurotransmitter currents on postsynaptic terminals. It validated through comparisons with the recent experimental findings. The results were incredibly well-matched to each other and this implies that small synapses might be conducted of dynamic functional modules and possibly hold the segregation of sites for spontaneous versus evoked neurotransmission within individual synapses.

2. We derived a finite difference approximation for solving the piecewise continuous heat equation in three dimensional space for a cubic domain, and proved its order of accuracy by numerical analysis. Then we also applied to the diffusion process and validated the method for the order of accuracy numerically. We concluded that for two finite difference schemes including consideration of the second order derivative correction across the interface by different diffusion constants, the overall error of the numerical methods should be second order.

10.3 Future Plan

We plan to continue our work refining our model how separation of NMDA receptors is distributed across individual synapses through more recent experimental findings. We consider electric field of synaptic currents that affect diffusion charged glutamate in synaptic cleft and improve of modeling by adopting earlier approach incorporating electric interaction between charged glutamate and receptor generated currents[58]. We apply our finite difference scheme in three dimensional for other elliptic equations with piecewise coefficients and compare with other works[30]. In addition, we study numerical methods such as Alternat-

ing Direction Implicit(ADI) method and find out if it is well suited for modeling of neural synapse[62].

From my perspective, I intend to continue my research in modeling for biological phenomena and developing numerical methods for biological modeling. I am fully ready for interdisciplinary research topics in other areas in science and engineering. Based on my solid mathematics and computation ability such as numerical differential equations, and statistical modeling, I look forward to new challenges in applied mathematics and work with other scientists in the frontier of science.

APPENDIX A

Polynomial Approximation and Interpolation

A.1 Piecewise-Polynomial Approximations

A piecewise-polynomial approximation is an alternative approximation to a single high order polynomial that may induce large fluctuations. This method is to divide the approximation interval into a collection of subinterval and construct a different approximating polynomial on each subinterval[7].

If we have a finite date set,

$$\{(x_0, f(x_0)), (x_1, f(x_1)), \cdots, (x_n, f(x_n))\}.$$

The simplest piecewise-polynomial approximation is piecewise-linear interpolation, which consists of joining a set of points by a series of straight line as shown black line with ∇ in Figure A.1. However, the function is not differentiable at the end of the subintervals, so the interpolating function is not smooth.

In order to compensate the weakness, we use another approximation that is a piecewise of Hermite type. If we know the values of f and f' are known at each of the points $x_0 < x_1 < \cdots < x_n$, a cubic Hermite polynomial can be used on each of the subintervals $[x_0, x_1], [x_1, x_2], \cdots, [x_{n-1}, x_n]$ to obtain a function that has a continuous derivative on the interval $[x_0, x_n]$. To use Hermite piecewise polynomials, it is required to obtain the derivative of the function being approximated, however, it is no easily availble.

The simplest differentiable piecewise-polynomial function on an entire interval is the functions by fitting one quadratic polynomial between each pair of nodes. However, we also need to specify the boundary condition at the end points x_0 and x_n.

The most common piecewise-polynomial approximation is to use cubic polynomial between a pair of points, this called cubic spline interpolation. A cubic polynomial involves four constants generally, so the function is smooth enough and the interpolant has a con-

tinuous second derivatives as well as continuously differentiable on the interval. The cubic spline interpolation satisfies the following.

Definition 4. *Given a function f defined on $[a, b]$ and a set of data points $a = x_0 < x_1 < \cdots < x_n = b$, a* **cubic spline interpolant** *R for f is a function that satisfies the following conditions.*

1. *$R(x)$ is a cubic polynomial, denoted $R_i(x)$, on the subinterval $[x_i, x_{i+1}]$ for each $i = 0, 1, \cdots, n-1$;*
2. *$R_i(x_i) = f(x_i)$ and $R_i(x_{i+1}) = f(x_{i+1})$ for each $i = 0, 1, \cdots, n-1$;*
3. *$R_{i+1}(x_{i+1}) = R_i(x_{i+1})$ for each $i = 0, 1, \cdots, n-2$;*
4. *$R'_{i+1}(x_{i+1}) = R'_i(x_{i+1})$ for each $i = 0, 1, \cdots, n-2$;*
5. *$R''_{i+1}(x_{i+1}) = R''_i(x_{i+1})$ for each $i = 0, 1, \cdots, n-2$;*
6. *One of the following sets of boundary condition is satisfied:*
   (a) *$R''(x_0) = R''(x_n) = 0$ (free boundary)*
   (b) *$R'(x_0) = f'(x_0)$ and $R'(x_n) = f'(x_n)$(clamped boundary).*

Since our simulation cost is expensive when we achieve the peak opening probability as a function of distant point on the postsynaptic terminal, we use cubic spline to find a smooth curve for the calculated data points as shown in Figure A.1.

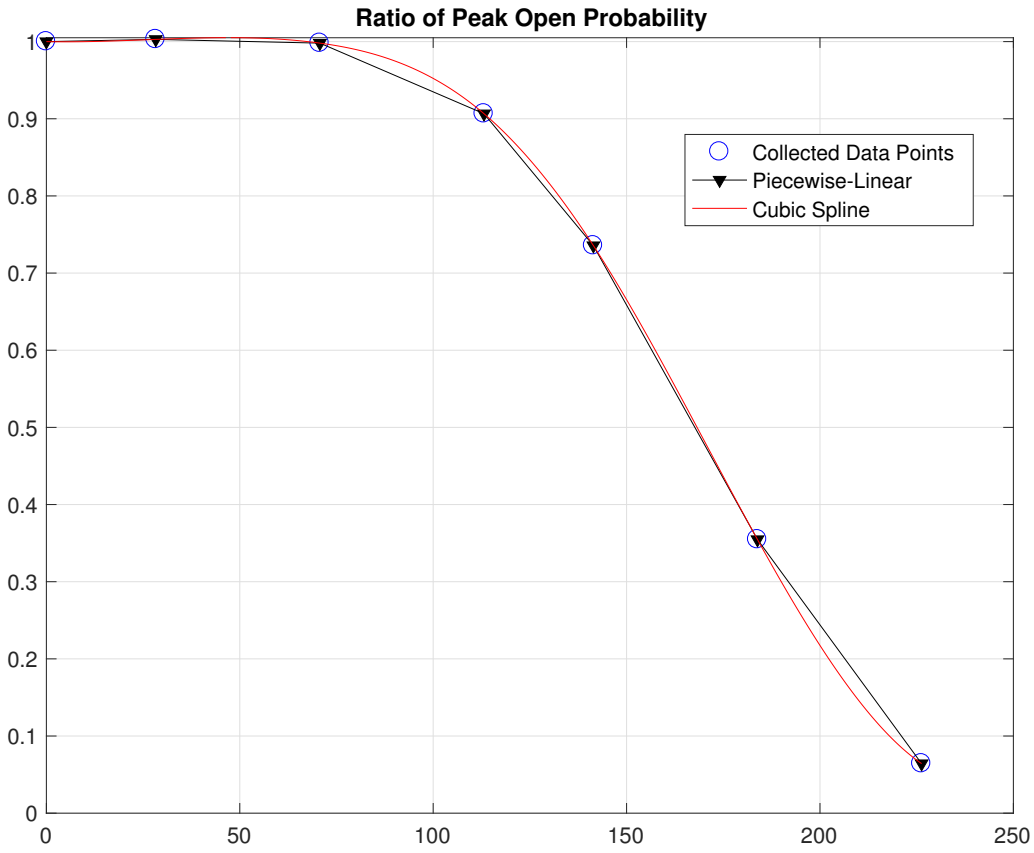

Figure A.1: This figure shows two ways to approximate a function based on known data points. Piecewise-linear approximation is simple but cubic spline interpolation is more smooth and continuously differentiable in the entire interval.

REFERENCES

[1] W. F. Ames. *Numerical Methods for Partial Differential Equations*. Academic Press, Inc., Boston, 3rd editio edition, 2014.

[2] L. C. Anson, P. E. Chen, D. J. Wyllie, D. Colquhoun, and R. Schoepfer. Identification of amino acid residues of the NR2A subunit that control glutamate potency in recombinant NR1/NR2A NMDA receptors. *Journal of Neuroscience*, 18(2):581–589, 1998.

[3] D. Atasoy, M. Ertunc, K. L. Moulder, J. Blackwell, C. Chung, J. Su, and E. T. Kavalali. Spontaneous and evoked glutamate release activates two populations of NMDA receptors with limited overlap. *Journal of Neuroscience*, 28(40):10151–10166, 2008.

[4] R. Bauerfeind, W. B. Huttner, W. Almers, and G. J. Augustin. Quantal neurotransmitter release from early endosomes? *Trends Cell Biology*, 4(May):155–156, 1994.

[5] P. Bogacki and L. F. Shampine. A 3(2) pair of Runge-Kutta formulas. *Applied Mathematics Letters*, 2(4):321–325, 1989.

[6] H. Brezis. *Functional Analysis, Sobolev Spaces and Partial Differential Equations*. Springer Science & Business Media, 2011.

[7] R. L. Burden and J. D. Faires. *Numerical Analysis*. Cengage Learning, 9th edition edition, 2011.

[8] D. J. Castillo and B. Katz. Quantal components of the end-plate potential. *Journal of Physiology*, 124:560–573, 1954.

[9] P. Chadderton, T. W. Margrie, and M. Häusser. Integration of quanta in cerebellar granule cells during sensory processing. *Nature*, 428(6985):856–860, 2004.

[10] J. D. Clements. Transmitter timecourse in the synaptic cleft: its role in central synaptic function. *Trends Neuroscience*, 19(96):163–171, 1996.

[11] M. Dehghan. Numerical solution of the three-dimensional advection-diffusion equation. *Applied Mathematics and Computation*, 150(1):5–19, 2004.

[12] J. S. Diamond and C. E. Jahr. Transporters buffer synaptically released glutamate on a submillisecond time scale. *Journal of Neuroscience*, 17(12):4672–4687, 1997.

[13] D. A. DiGregorio, Z. Nusser, and R. A. Silver. Spillover of glutamate onto synaptic AMPA receptors enhances fast transmission at a cerebellar synapse. *Neuron*, 35(3):521–533, 2002.

[14] A. Einstein. Über die von der molekularkinetischen theorie der wärme geforderte bewegung von in ruhenden flüssigkeiten suspendierten teilchen. *Annalen der physik*, 322(8):549–560, 1905.

[15] L. C. Evans. *Partial Differential Equations*. American Mathematical Society, 2nd edition, 2010.

[16] R. Ewing, O. Iliev, and R. Lazarov. A modified finite volume approximation of second-order elliptic equations with discontinuous coefficients. *SIAM Journal on Scientific Computing*, 23(4):1335–1351, 2001.

[17] P. Fatt and B. Katz. Spontaneous subthreshold activity at motor nerve endings. *Journal of Physiology*, 117:109–128, 1951.

[18] M. Frerking and M. Wilson. Saturation of postsynaptic receptors at central synapses ? *Current Opinion in Neurobiology*, 6:395–403, 1995.

[19] M. Geppert, Y. Goda, R. E. Hammer, C. Li, T.W. Rosahl, C. F. Stevens, and T. C. Südhof. Synaptotagmin I: a major Ca2+ sensor for transmitter release at a central synapse. *Cell*, 79(4):717–727, 1994.

[20] S. M. Hill. Receptor crosstalk: communication through cell signaling pathways . *The Anatomical record*, 253(2):42–48, 1998.

[21] J. M. Hyman. Accurate monotonicity preserving cubic interpolation. *SIAM Journal on Scientific and Statistical Computing*, 4(4):645–654, 1983.

[22] J. S. Isaacson and B. Walmsley. Counting quanta: direct measurements of transmitter release at a central synapse. *Neuron*, 15:875–884, 1995.

[23] A. Iserles. *A First Course in the Numerical Analysis of Differential Equations*. Cambridge Univerisity Press, (1996).

[24] E. T. Kavalali. *Nature Reviews. Neuroscience*, 16(1):5–16, 2014.

[25] E. T. Kavalali, C. Chung, M. Khvotchev, J. Leitz, E. Nosyreva, J. Raingo, and D. Ramirez. Spontaneous neurotransmission: an independent pathway for neuronal signaling? *Physiology (Bethesda, Md.)*, 26(1):45–53, 2011.

[26] J. Keener and J. Sneyd. *Mathematical Physiology*. Springer Science & Business Media, New York, 2nd edition, 2004.

[27] A. Kenny, N. R. B. Cary, D. Murphy, and L. M. Shapiro. Intraoperative epicardial echocardiography with a miniature high-frequency transducer: imaging techniques and Scanning Planes. *Journal of the American Society of Echocardiography*, 7(2):141–149, 1994.

[28] J. LeDoux. *Synaptic Self: How Our Brains Become Who We Are*. Penguin Publishing Group, 2003.

[29] R. J. LeVeque. *Finite Difference Methods for Ordinary and Partial Differential Equations*. Society for Industrial and Applied Mathematics (SIAM), Philadelphia, 2007.

[30] R. J. LeVeque and Z. Li. Immersed interface methods for elliptic equations with discontinuous coefficients and singular source. *SIAM Journal of Scientific Computing*, 31(4):1019–1044, 1994.

[31] H. Lewy, K. Friedrichs, and R. Courant. Uber die partiellen differenzengleichungen der mathematischen physik. *Mathematische Annalen*, 100:32–74, 1928.

[32] Z. Li. *The immersed interface method - a numerical approach for partial differential equations with interfaces*. PhD thesis, University of Washington, 1994.

[33] Z. Li. A note on immersed interface method for three-dimensional elliptic equations. *Computers & Mathematics with Applications*, 31(3):9–17, 1996.

[34] Z. Li and Y. Shen. A numerical method for solving heat equations involving interfaces. *Fourth Mississippi State Conference on Differential Equations and Computational Simulation, Electronic Journal of Differential Equations, Conference 03*, pages 100–108, 1999.

[35] J. K. Liu and Z. S. Zheng. Efficient high-order immersed interface methods for heat equations with interfaces. *Applied Mathematics and Mechanics (English Edition)*, 35(9):1189–1202, 2014.

[36] The Mathworks, Inc., Natick, Massachusetts. *MATLAB version 8.5.0.197613 (R2015a)*, 2015.

[37] A. Mayor. The fast solution of Possion's and the Biharmonic equations on irregular regions. *SIAM Journal on Numerical Analysis*, 21(2):285–299, 1984.

[38] J. E. Melom, Y. Akbergenova, J. P. Gavornik, and J. T. Littleton. Spontaneous and evoked release are independently regulated at individual active zones. *Journal of Neuroscience*, 33(44):17253–17263, 2013.

[39] K.W. Morton and D. Mayers. *Numerical Solution of Partial Differential Equations*. Cambridge Univerisity Press, Cambridge, 2005.

[40] V. N. Murthy and C. F. Stevens. Synaptic vesicles retain their identity through the endocytic cycle. *Nature*, 392(6675):497–501, 1998.

[41] T. A. Nielsen, D. A. DiGregorio, and R. A. Silver. Modulation of glutamate mobility reveals the mechanism underlying slow-rising AMPAR EPSCs and the diffusion coefficient in the synaptic cleft. *Neuron*, 42(5):757–771, 2004.

[42] Y. Otsu and T. H. Murphy. Miniature transmitter release: accident of nature or careful design? *Science's STKE : signal transduction knowledge environment*, (211):54, 2003.

[43] D. Paré, E. Lebel, and E. J. Lang. Differential impact of miniature synaptic potentials on the soma and dendrites of pyramidal neurons in vivo. *Journal of Neurophysiology*, 78(3):1735–1739, 1997.

[44] D. Paré, E. Shink, H. Gaudreau, A. Destexhe, and E. J. Lang. Impact of spontaneous synaptic activity on the resting properties of cat neocortical pyramidal neurons In vivo. *Journal of Neurophysiology*, 79(3):1450–1460, 1998.

[45] D. K. Patneau and M. L. Mayer. Structure-activity relationships for amino acid transmitter candidates acting at N-methyl-D-aspartate and quisqualate receptors. *Journal of Neuroscience*, 10(7):2385–2399, 1990.

[46] E. S. Peled, Z. L. Newman, and E. Y. Isacoff. Evoked and spontaneous transmission favored by distinct sets of synapses. *Current Biology*, 24(5):484–493, 2014.

[47] G. Popescu, A. Robert, J. R. Howe, and A. Auerbach. Reaction mechanism determines NMDA receptor response to repetitive stimulation. *Nature*, 430(7001):790–793, 2004.

[48] G. W. Recktenwald. *Numerical Methods with MATLAB: Implementations and Applications*. Prentice-Hall, Upper-Saddle River, NJ, 2000.

[49] A. L. Reese and E. T. Kavalali. Single synapse evaluation of the postsynaptic NMDA receptors targeted by evoked and spontaneous neurotransmission. *eLife*, 5:e21170, 2016.

[50] Y. Sara, T. Virmani, F. Deák, X. Liu, and E. T. Kavalali. An isolated pool of vesicles recycles at rest and drives spontaneous neurotransmission. *Neuron*, 45(4):563–573, 2005.

[51] C. Saviane and R. A. Silver. Fast vesicle reloading and a large pool sustain high bandwidth transmission at a central synapse. *Nature*, 439(7079):983–987, 2006.

[52] R. Schneggenburger and C. Rosenmund. Molecular mechanisms governing Ca(2+) regulation of evoked and spontaneous release. *Nature Neuroscience*, 18(7):935–941, 2015.

[53] S. B. Seo, J. Su, E. T. Kavalali, and J. Blackwell. Quantifying the constraints for independent evoked and spontaneous NMDA receptor mediated synaptic transmission at individual synapses, 25th Annual Computational Neuroscience Meeting: CNS-2016. *BMC Neuroscience*, 17(1):196, 2016.

[54] L. F. Shampine and M. W. Reichelt. The MATLAB ODE Suite. *SIAM Journal on Scientific Computing*, 18(1):1–22, 1997.

[55] M. J. Shashkov and S. Steinberg. Solving diffusion equations with rough coefficients in rough grids. *Journal of Computational Physics*, 129(2):383–405, 1996.

[56] T. C. Südhof and J. Rizo. Synaptic vesicle exocytosis. *Cold Spring Harbor perspectives in biology*, 3(12):1–14, 2011.

[57] M. A. Sutton, N. R. Wall, G. N. Aakalu, and E. M. Schuman. Regulation of dendritic protein synthesis by miniature synaptic events. *Science (New York, N.Y.)*, 304(5679):1979–1983, 2004.

[58] S. Sylantyev, L. P. Savtchenko, Y. Ermolyuk, P. Michaluk, and D. A. Rusakov. Spike-driven glutamate electrodiffusion triggers synaptic potentiation via a homer-dependent mGluR-NMDAR Link. *Neuron*, 77(3):528–541, 2013.

[59] A. H. Tang, H. Chen, T. P. Li, S. R. Metzbower, H. D. MacGillavry, and T. A. Blanpied. A trans-synaptic nanocolumn aligns neurotransmitter release to receptors. *Nature*, 536(7615):210–4, 2016.

[60] M. J. Wall and M. M. Usowicz. Development of the quantal properties of evoked and spontaneous synaptic currents at a brain synapse. *Nature Neuroscience*, 1:675–682, 1998.

[61] D. Zenisek. Vesicle association and exocytosis at ribbon and extraribbon sites in retinal bipolar cell presynaptic terminals. *Proceedings of the National Academy of Sciences of the United States of America*, 105(12):4922–4927, 2008.

[62] S. Zhao. A matched alternating direction Implicit (ADI) method for solving the heat equation with interfaces. *Journal of Scientific Computing*, 63(1):118–137, 2015.

[63] R. S. Zucker. Minis: whence and wherefore? *Neuron*, 45(4):481–482, 2005.

BIOGRAPHICAL STATEMENT

Sat byul Seo was born in December 9 in 1986, in Changwon, South Korea. She majored in Mathematics Education and received her B.S. degree from Kyungnam University, South Korea in 2009. Then she moved to United States, and continued her study for Applied Mathematics. She obtained her M.S. and Ph.D. degrees from The University of Texas at Arlington in 2015 and 2017, respectively, all in Mathematics.